PLANT CELL

Research Article

F-actin regulates the polarized secretion of pollen tube attractants in Arabidopsis synergid cells

Daichi Susaki [ID],[1] Rie Izumi [ID],[1] Takao Oi [ID],[2] Hidenori Takeuchi [ID],[3,4] Ji Min Shin [ID],[5] Naoya Sugi [ID],[1] Tetsu Kinoshita [ID],[1] Tetsuya Higashiyama [ID],[3,6,7] Tomokazu Kawashima [ID][5] and Daisuke Maruyama [ID][1,*]

1   Kihara Institute for Biological Research, Yokohama City University, Maioka-cho 641-12, Totsuka-ku, Yokohama, Kanagawa, 244-0813, Japan
2   Graduate school of Bioagricultural Sciences, Nagoya University, Furo-cho, Chikusa-ku, Nagoya, Aichi 464-8602, Japan
3   Institute of Transformative Bio-Molecules (WPI-ITbM), Nagoya University, Furo-cho, Chikusa-ku, Nagoya, Aichi 464-8601, Japan
4   Institute for Advanced Research, Nagoya University, Furo-cho, Chikusa-ku, Nagoya, Aichi 464-8601, Japan
5   Department of Plant and Soil Sciences, University of Kentucky, 321 Plant Science Building, Lexington, Kentucky 40546, USA
6   Division of Biological Science, Graduate School of Science, Nagoya University, Furo-cho, Chikusa-ku, Nagoya, Aichi 464-8602, Japan
7   Department of Biological Sciences, Graduate School of Science, The University of Tokyo, Hongo, Bunkyo-ku, Tokyo 113-0033, Japan

*Author for correspondence: dmaru@yokohama-cu.ac.jp

D.M. and T. Ka. conceived this project; D.S. obtained confocal images in Figures 1 and 2, Supplemental Figures 1–4 and Supplemental Movies 2–5; T.O. conducted FIB-SEM analysis and image processing in Figure 1 and Supplemental Movie 1; J.M.S., T. Ka., analyzed F-actin dynamics and colocalization analysis of F-actin and microtubule in Figure 2, Supplemental Figure 2. R.I. and D.M. analyzed fertility of DN-ACTIN expressing lines; R.I and H.T. contributed immunostaining in Supplemental Figure 2; N.S. analyzed the invagination length in Figure 1; D.M. obtained other data and directed this project; D.M. and D.S. wrote the manuscript and all authors contributed to edit the manuscript.
The author responsible for distribution of materials integral to the findings presented in this article in accordance with the policy described in the Instructions for Authors (https://academic.oup.com/plcell/pages/General-Instructions) is: Daisuke Maruyama (dmaru@yokohama-cu.ac.jp).

Abstract

Pollen tube attraction is a key event of sexual reproduction in flowering plants. In the ovule, two synergid cells neighboring the egg cell control pollen tube arrival via the active secretion of attractant peptides such as AtLURE1 and XIUQIU from the filiform apparatus (FA) facing toward the micropyle. Distinctive cell polarity together with longitudinal F-actin and microtubules are hallmarks of the synergid cell in various species, though the functions of these cellular structures are unclear. In this study, we used genetic and pharmacological approaches to indicate the roles of cytoskeletal components in FA formation and pollen tube guidance in *Arabidopsis thaliana*. Genetic inhibition of microtubule formation reduced invaginations of the plasma membrane but did not abolish micropylar AtLURE1.2 accumulation. By contrast, the expression of a dominant-negative form of ACTIN8 induced disorganization of the FA and loss of polar AtLURE1.2 distribution toward the FA. Interestingly, after pollen tube reception, F-actin became unclear for a few hours in the persistent synergid cell, which may be involved in pausing and resuming pollen tube attraction during early polytubey block. Our data suggest that F-actin plays a central role in maintaining cell polarity and in mediating male–female communication in the synergid cell.

Introduction

Sexual plant reproduction proceeds with multicellular haploid tissues termed gametophytes. Most flowering plants, including *Arabidopsis thaliana*, produce a *Polygonum*-type female gametophyte that contains seven cells: one egg cell, one central cell, two synergid cells, and three antipodal cells. By contrast, pollen grains or pollen tubes are the male gametophytes and contain fewer cells, with a tip-growing pollen tube vegetative cell that contains two sperm cells. Sexual reproduction is accomplished when the egg cell and central cell are fertilized by two sperm cells delivered by the pollen tube. Although the synergid cell itself is not fertilized, it is responsible for many communications between female and male gametophytes prior to double fertilization. The synergid cell controls pollen tube

IN A NUTSHELL

Background: The two synergid cells embedded in the ovule of angiosperms play an important role in the male–female interaction during sexual reproduction by secreting pollen tube attractants (e.g. AtLUREs). The micropylar end of a synergid cell has a filiform apparatus (FA), active communication domain with complex plasma membrane invaginations and thick cell walls that presumably secrete the attractant peptides. Immunostaining studies have shown radial microtubules spreading from the FA and filamentous actin (F-actin) distributed longitudinally within the synergids. The characteristic morphology and cytoskeletal orientation of synergid cells are thought to be important for their function, but the details are unclear.

Question: What is the function of the cytoskeleton in synergid cells during sexual reproduction?

Findings: We demonstrated that microtubule destruction compromises the elongation of plasma membrane invaginations in the FA. Disruption of F-actin resulted in severe disorganization of synergid cell morphology, causing incomplete FA formation and aberrant positioning of the central vacuole. Furthermore, F-actin destruction impaired the secretion of pollen tube attractant peptides and caused female sterility. After pollen tube discharge, the longitudinal F-actin pattern temporarily disappeared in the persistent synergid. Our data suggest that F-actin has a central role in maintaining cell polarity and in mediating male–female communication in the synergid cell.

Next step: The genes that regulate the polar secretion and cell morphology of synergid cells remain to be identified in further studies. Such studies will further our understanding of the mechanisms that underlie pollen tube attraction and polytubey block, the process by which the ovule limits the number of pollen tubes it attracts.

attraction, pollen tube reception, termination of pollen tube attraction, and fertilization recovery (Dresselhaus et al., 2016).

In the past two decades, many synergid cell-specific genes have been identified that are required for the communication between the female and male gametophytes. In some species, various pollen tube attractants secreted from the filiform apparatus (FA) of the synergid cell have been identified: ZmEA1 in maize (Marton et al., 2005, 2012); LURE1 and LURE2 in *Torenia* (Okuda et al., 2009); AtLURE1s, XIUQIUs, and TICKETs in *A. thaliana* (Takeuchi and Higashiyama, 2012; Meng et al., 2019; Zhong et al., 2019). Receptor-like kinases on the pollen tube tip, including PRK6, interact with AtLURE1 and control the directional growth of the pollen tube (Takeuchi and Higashiyama, 2016). After arrival of the pollen tube, one of the two synergid cells receives the pollen tube contents, including the two sperm cells. The receptive synergid regulates pollen tube discharge via CrRLK1L-type receptor-like kinases such as FERONIA, ANJEA, and HERCULES RECEPTOR KINASE 1 (HERK1) (Escobar-Restrepo et al., 2007; Galindo-Trigo et al., 2020), a GPI-anchored protein LORELEI (Capron et al., 2008; Tsukamoto et al., 2010), and a Mildew resistance locus o (MLO) family-related protein NORTIA (Kessler et al., 2010). Genetic and biochemical approaches have begun to uncover their cooperative mechanisms during pollen tube reception (Li et al., 2015; Ju et al., 2021). Following pollen tube reception, ovules prevent the attraction of extra pollen tubes, a process called polytubey block, reducing risk of egg cell fertilization by more than one sperm cell known as polyspermy (Beale et al., 2012; Kasahara et al., 2012; Maruyama and Higashiyama, 2016). In early ovular polytubey block, activated just before or upon double fertilization, synergid cells produce nitric oxide (NO) in a FERONIA-dependent manner. The NO signal not only inactivates AtLURE1 peptides via post-translational nitrosation, but also inhibits the AtLURE1 secretory system by an unknown mechanism (Duan et al., 2020). In addition, the clearance of attractants may be accelerated by fertilization-dependent secretion of aspartic endopeptidases from the zygote (Yu et al., 2021). On the other hand, later stages of the polytubey block are initiated a few hours after double fertilization by the inactivation of the non-receptive persistent synergid. Representative features of the persistent synergid elimination are nuclear degeneration and cell-to-cell fusion between the persistent synergid and the endosperm (Maruyama et al., 2013, 2015; Völz et al., 2013; Pereira et al., 2016). If ovules are not fertilized by the first pollen tube, they pause the degeneration of the persistent synergid and resume the attraction of the next pollen tube (Beale et al., 2012; Kasahara et al., 2012).

The synergid cell displays a highly polarized morphology, characterized by the concentration of the protoplasm at the micropylar side, facing toward the pollen tube entry pathway in the ovule, and a large central vacuole at the opposite chalazal side (Mansfield et al., 1991). The micropylar end of the synergid cell has the FA, an active communication domain with complex plasma membrane invaginations and thick cell walls, that presumably has pivotal roles in secreting sufficient concentration of pollen tube attractant peptides and localizing pollen tube reception factors (Johnson et al., 2019). Synergid cell shape formation and dynamic protein relocation or secretion may be regulated by the cytoskeleton. Immunostaining studies have shown radial microtubules spreading from the FA in various species including *A. thaliana* (Webb and Gunning, 1994). By contrast, filamentous actin (F-actin) is widely distributed longitudinally along the micropyle–chalazal axis (Webb and Gunning, 1994). However, the significance of the cytoskeleton in synergid cells remains unclear.
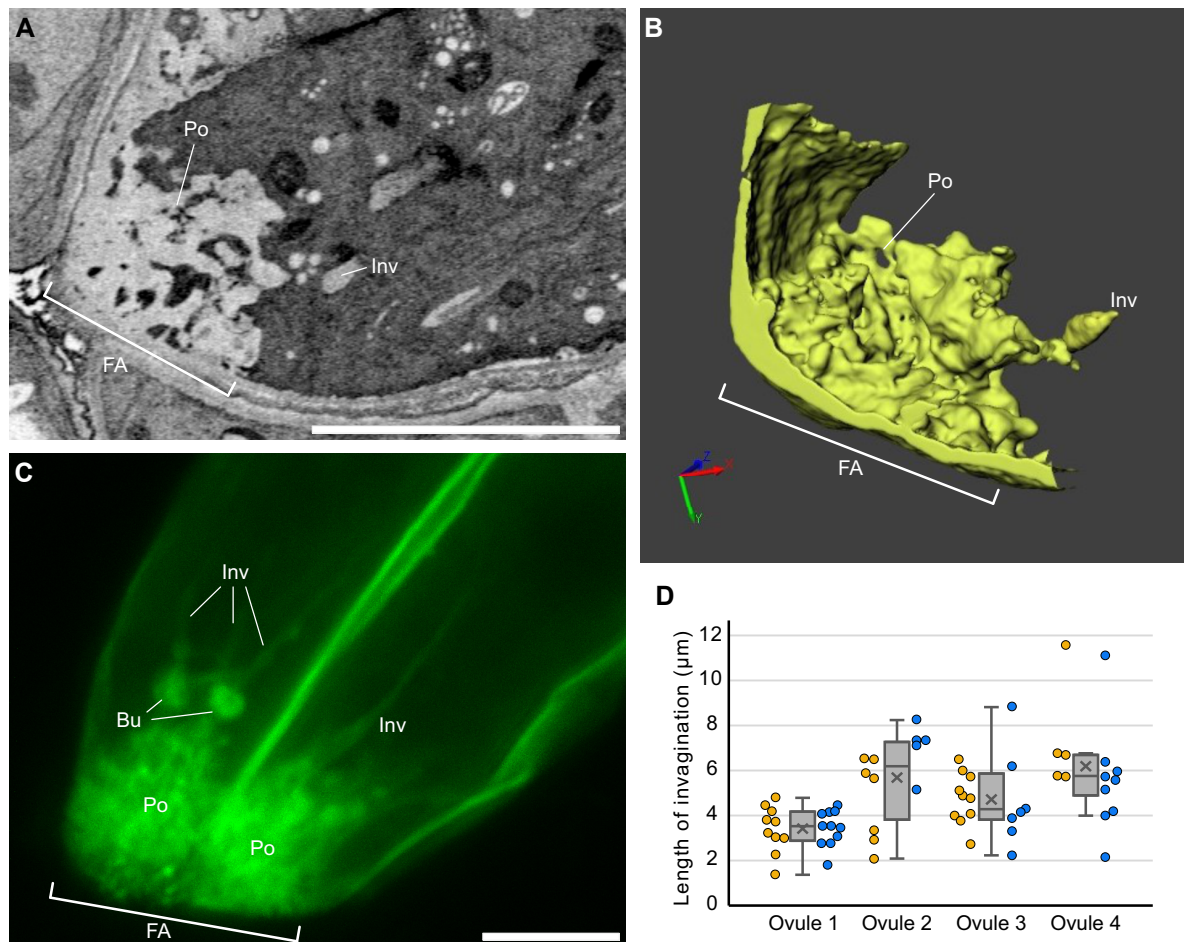
Figure 1 Morphology of the FA in *Arabidopsis thaliana*. A, B, FA analyzed by FIB-SEM (See also Supplemental Movie 1). A single plane selected from the serial section (A). 3D reconstruction image of the synergid cell wall (B). C, Plasma membrane pattern observed in a T2 *ProMYB98:3×mNG-SYP132* synergid cell. A maximum intensity projection from the selected Z-serial sequences in Supplemental Movie 2 is shown. D, Length of plasma membrane invaginations at the FA in *ProMYB98:3×mNG-SYP132* plants. Box-and-whisker plots show median (center line), mean (cross mark), upper and lower quartiles (box), maximum and minimum (whiskers), and left and right points corresponding the data from each synergid cell. Abbreviations: FA, filiform apparatus; Po, porous structure; Inv, invagination; Bu, bulge. Scale bars: 5 μm in (A) and (C).

In this study, we aimed to investigate the functions of the cytoskeleton in *A. thaliana* synergid cells. We used genetic and pharmacological approaches to induce microtubule- and actin-depolymerization. Our results indicate that microtubule destruction compromises the elongation of plasma membrane invaginations in the FA. By contrast, disruption of F-actin caused severe disorganization of synergid cell morphology, including phenotypic alterations such as incomplete FA formation and aberrant positioning of the central vacuole. Furthermore, F-actin destruction impaired the secretion of pollen tube attractant peptides and caused female sterility. Interestingly, the longitudinal F-actin pattern disappeared in the persistent synergid after pollen tube discharge, suggesting that F-actin is dynamically regulated during fertilization. Altogether, these findings elucidate the flexibility of the F-actin-mediated directional secretion system that maintains the morphology and function of the synergid cell.

Results

Morphology of the FA

The FA has usually been described as a finger-like structure based on observations of mature ovules by transmission electron microscopy (Jensen, 1965; Diboll and Larson, 1966; Schulz and Jensen, 1968). To update our knowledge of the FA morphology, we conducted a three-dimensional (3D) reconstruction of a mature *A. thaliana* ovule by focused ion beam-scanning electron microscopy (FIB-SEM) (Oi et al., 2017). A 3D image reconstructed from the serial sections (713 sequential electron micrographs with 25 nm step size) showed a sponge-like porous domain (Po) of cell walls at the micropylar end of the FA, rather than the finger-like pattern that is often used to depict the FA in 2D electron micrographs (Figure 1, A and B; Supplemental Movie 1). According to the 3D model, the surface area of the FA was 3.7-fold larger than the presumed cell wall area excluding invaginations (72.3 μm^2 and 19.8 μm^2, respectively).

Next, we generated a plasma membrane marker *ProMYB98:3×mNG-SYP132*, expressing Syntaxin of plant 132 (SYP132) tagged with tandem fusions of three mNeonGreen fluorescent proteins driven by the synergid cell-specific *MYB98* promoter (Uemura et al., 2004; Kasahara et al., 2005; Shaner et al., 2013) and analyzed complex structures of the FA in live synergid cells by confocal microscopy (Figure 1C; Supplemental Movie 2). Z-series confocal images showed that the porous structure exhibited strong fluorescent signals due to the accumulations of vesicular- or folded-plasma membranes (Figure 1C and Supplemental Figure 1C, Po). In contrast to the FIB-SEM data, we observed long protrusions of the tubular plasma membrane from the porous area toward the inside of the cell (Figure 1C and Supplemental Figure 1C, Inv). Among the eight synergid cells in the four ovules, we observed an average of 8.0 ± 2.3 invaginations per cell with a length ranging from 1.8 to 11.5 μm (Figure 1D). The size of the invagination was comparable between pairs of synergid cells from the same ovule but varied among different ovules (Figure 1D). In addition, bulges were observed along the invaginations in three ovules (Figure 1C, Bu). Cell wall staining with SCRI Renaissance Stain 2200 (Musielak et al., 2015) in the *ProES2:3×mNG-SYP132* (ENS) plasma membrane marker revealed that the cell wall and plasma membrane in live synergid cells showed reciprocally complemented patterns including long invaginations and micropylar spongy-like structures (Supplemental Figure 1C).

Morphology and dynamics of the cytoskeleton in the synergid cell

The formation of complex plant cell morphologies often requires F-actin and/or microtubules (Eng and Sampathkumar, 2018). To investigate the pattern of these cytoskeleton filaments in the live synergid cell, we generated a double marker line expressing an F-actin binding Lifeact peptide tagged with mRUBY3 (Lifeact-mRUBY3) and TUBULIN ALPHA 5 fused with Citrine (Citrine-TUA5) from the synergid cell-specific *MYB98* promoter (Kasahara et al., 2005; Riedl et al., 2008; Shaner et al., 2013). In the mature ovules, mRUBY3 signal of F-actin extended from the micropylar end, where the FA resides, and reached beyond synergid nuclei and large central vacuoles to the chalazal end (Figure 2A, left panel). Citrine-labeled microtubules were also longitudinally aligned around the FA, forming a radially extended cat-whisker pattern (Figure 2A, middle panel), where F-actin often associated or co-localized with microtubules (Figure 2A, right panel).

In the egg cell and central cell, F-actin is generated at the cell periphery and migrates toward the nucleus, supporting the rapid merger of female and male nuclei (karyogamy) after gamete fusion (plasmogamy) (Kawashima et al., 2014; Ohnishi et al., 2014; Ohnishi and Okamoto, 2015). To examine whether fertilization-incompetent gametophytic cells (i.e. synergid cells) have the similar nucleopetal F-actin dynamics,

we observed F-actin dynamics in the synergid cells of mature ovules (*ProMYB98:Lifeact-mNG*) by time-lapse imaging at 30 s intervals. The movie showed that actin cables actively moved longitudinally (Supplemental Movie 3), and we further performed a spatiotemporal image correlation spectroscopy analysis (Ashdown et al., 2015) to evaluate the directions of F-actin flow at four areas (two in the chalazal and one each in peri-nuclear and micropylar regions). Radar plots indicated that the directions of F-actin flow were mainly from chalazal to micropyle, except for in the micropylar region (Figure 2, B–E and Supplemental Figure 2). Around the FA, the F-actin flow was omnidirectional, implying active rearrangements of F-actin. These results show that, unlike the nucleopetal F-actin dynamics of the gametes, overall F-actin dynamics in the synergid cell are toward the FA.

Genetic disruption of microtubule formation

To analyze the roles of microtubules in the synergid cell, we used PHS1ΔP, a dominant mutant of PROPYZAMIDE-HYPERSENSITIVE 1 (PHS1). PHS1 is an α-tubulin kinase consisting of a central tubulin kinase domain and a C-terminal phosphatase domain (Fujita et al., 2013). PHS1ΔP lacks the C-terminal phosphatase domain and shows high tubulin kinase activity, inducing microtubule depolymerization via overproduction of polymerization-inefficient phosphorylated α-tubulins (Fujita et al., 2013). We generated two transgenic lines homozygous for a transgene expressing *PHS1ΔP* from the *MYB98* promoter (*ProMYB98:PHS1ΔP*) that were also homozygous for two reporter genes visualizing synergid cell morphology: *ProRPS5A:H2B-tdTomato* (RHT) and *ProES2:3×mNG-SYP132* (ENS). RHT is a nuclear marker expressing tdTomato-tagged HISTONE H2B from the ubiquitously active *Ribosomal Protein Subunit 5A* promoter (Maruyama et al., 2013). As shown in Supplemental Figure 1, ENS is a plasma membrane marker expressing 3×mNeonGreen-SYP132 from the embryo sac-specific *ES2* promoter (Yu et al., 2005; Pagnussat et al, 2007).

The mature ovules from the *ProMYB98::PHS1ΔP*; RHT; ENS transgenic lines were compared with those from the wild-type RHT; ENS line using confocal microscopy. In wild-type RHT; ENS, 97.7% of the ovules contained the normal seven-celled female gametophyte with two synergid cells, an egg cell, a central cell, and three antipodal cells (Figure 3A, $n = 386$). On the other hand, in *ProMYB98:PHS1ΔP*; RHT; ENS, only 9.3%–12.9% of the gametophytes showed a normal cell structure (Figure 3B, Two synergids; Figure 3F), and the remaining ovules exhibited various aberrations. Specifically, 37.2%–37.5% of the ovules contained a single-synergid cell with either one or two nuclei (Figure 3C, single synergid). Because the *MYB98* promoter becomes active prior to cellularization of the eight-nucleate female gametophyte (Kasahara et al., 2005; Susaki et al., 2021), these single-synergid ovules were likely generated due to the inadequate spindle and/or cell plate formation caused by PHS1ΔP-mediated microtubule depolymerization (Figure 3, C and F, SY-SY fusion). Consistently, we observed more severe phenotypes in *ProMYB98:PHS1ΔP*; RHT; ENS;
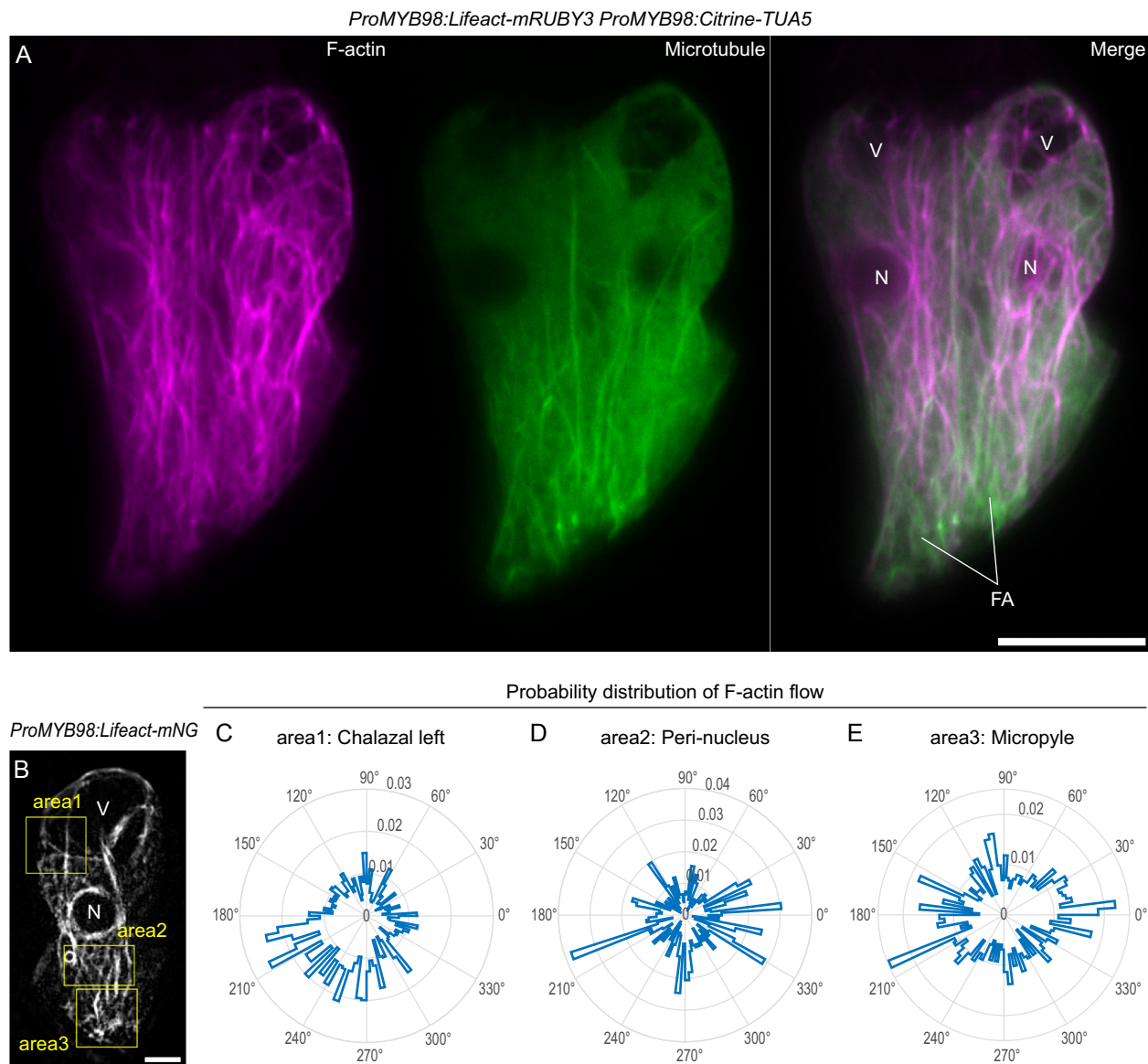
Figure 2 Distribution of cytoskeleton filaments in synergid cells. A, Maximum intensity projection confocal images of a pair of synergid cells expressing the *Lifeact-mRUBY3* F-actin marker and *Citrine-TUA5* microtubule marker from the *MYB98* promoter. B, The first frame of time-lapse imaging of F-actin dynamics in the synergid cell. A mature ovule in the transgenic plant expressing the *Lifeact-mNeonGreen* F-actin marker from the *MYB98* promoter (*ProMYB98:Lifeact-mNG*) was captured in 30 s intervals. The yellow boxes indicate the areas where F-actin flow was analyzed as shown in (C–E). V, vacuole; N, nucleus; FA, filiform apparatus; Scale bars, 10 μm in (A) and (B). C–E, Radar plots showing probability distributions of the directions of F-actin flow vectors in each area (the box in (B)) obtained via spatiotemporal image correlation spectroscopy analysis. The probability was calculated from cumulative frequency of the F-actin flow vector angles obtained from the entire frames of time-lapse imaging. The probability values are scaled in the radial axes on the radar plots.

including the disappearance of mNeonGreen-labeled plasma membrane accumulation, a hallmark of the FA, in 49.5%–53.6% of the ovules (Figure 3, D and E, No FA). Occasionally, these ovules contained no nuclei in the putative synergid region while the central cell had multiple nuclei (Figure 3E, 9.5%–10.3%). To monitor female gametogenesis, we cultured immature ovules in a liquid medium and performed live imaging. In the wild-type *RHT; ENS* line, two synergid nuclei were localized at the micropylar end throughout female gametogenesis (Supplemental Figure 3A; Supplemental Movie 4: $n = 24$). However, we observed that the synergid nucleus (or two synergid nuclei) migrated toward the central cell and participated in the fusion of polar nuclei during cellularization of eight-nucleated female gametophytes in *ProMYB98:PHS1ΔP; RHT; ENS* (Supplemental Figure 3B and Movie 5; migration of single nucleus, $n = 33$; migration of both nuclei $n = 13$).
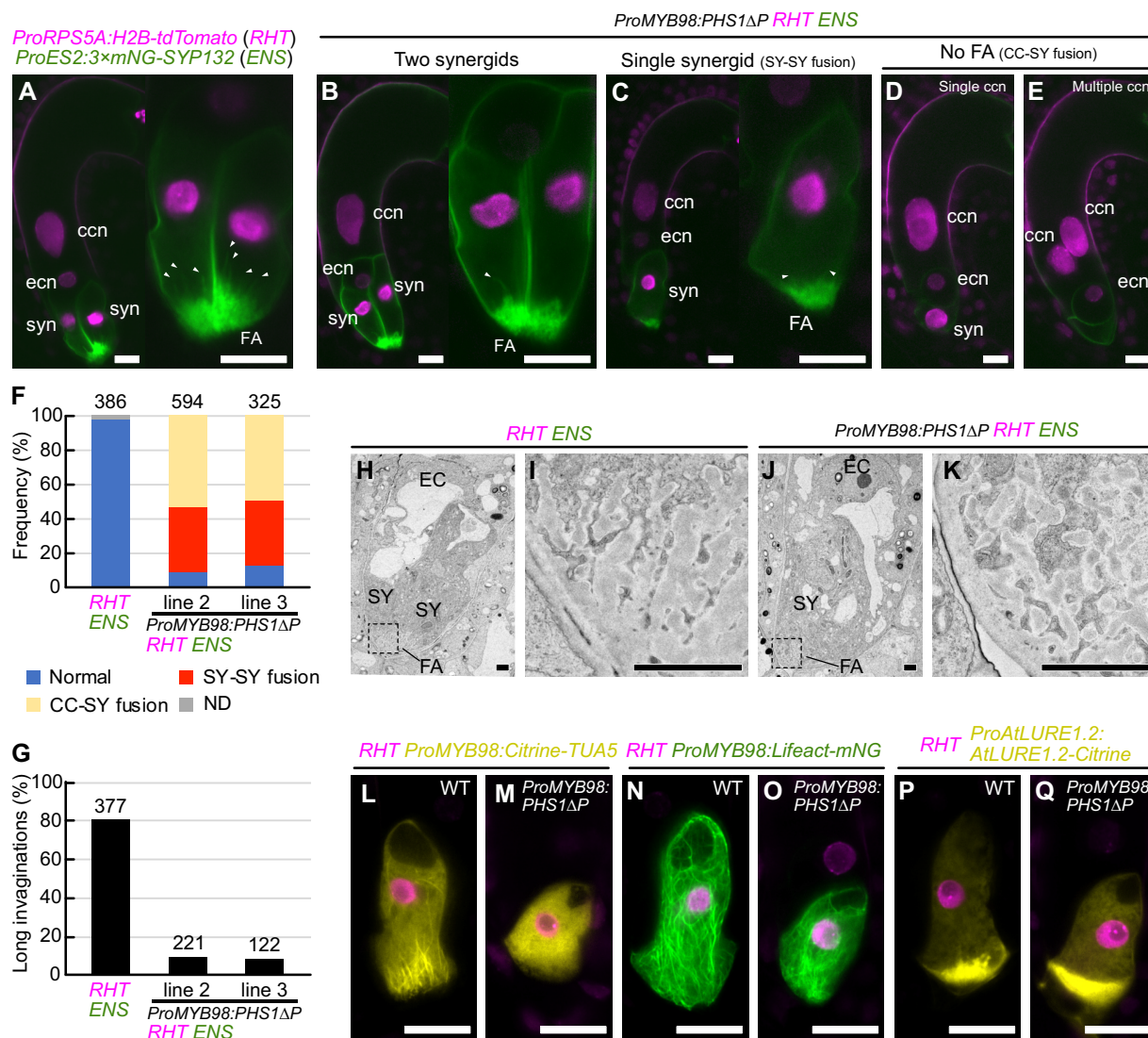
Figure 3 Genetic disruption of microtubules using a synergid-specific promoter. A, Wild-type ovule carrying the nuclear marker (*RHT*) and plasma membrane marker (*ENS*). B–E, Ovules containing two synergid cells (B), single-synergid cell (C), a single central cell nucleus without FA (D), or multiple central cell nuclei without a FA (E) observed in the *RHT; ENS* double marker line that were also homozygous for the microtubule destruction gene *PHS1ΔP* expressed from the *MYB98* promoter (*ProMYB98:PHS1ΔP*). In (A–C), the synergid cell(s) in the left panel is magnified and shown in the right panel. White arrowheads indicate the plasma membrane invagination. F, G, Frequency of normal and aberrant female gametophyte (F) and percentages of FA with long invaginations (G) in wild-type *RHT; ENS* line and two *ProMYB98:PHS1ΔP; RHT; ENS* lines. The numbers above the bars indicate total ovules. H–K, Transmission electron micrographs of wild-type ovule in the *RHT; ENS* line (H) and single-synergid cell-containing ovule of the *ProMYB98:PHS1ΔP; RHT; ENS* line (J). Magnification of areas of the FA indicated with dashed boxes in (H) and (J) are shown in (I) and (K), respectively. L–Q, Confocal images of synergid cells expressing *RHT* nuclear marker and other reporter genes showing synergid cell structures in wild-type plants (L, N, P) and *ProMYB98:PHS1ΔP* transgenic lines (M, O, Q). The synergid cell-specific reporters were as follows: *ProMYB98:Citrine-TUA5* (microtubules; L, M), *ProMYB98:Lifeact-mNG* (F-actin; N, O), *ProAtLURE1.2:AtLURE1.2-Citrine* (pollen tube attractant; P, Q). Abbreviations: *RHT*, *ProRPS5A:H2B-tdTomato*; *ENS*, *ProES2:3×mNG-SYP132*; ccn, central cell nucleus; ecn, egg cell nucleus; syn, synergid cell nucleus; FA, FA; SY, synergid cell; EC, egg cell; CC, central cell. Scale bars: 20 µm in (A) to (E) and (L) to (Q); 2 µm in (H) to (K).

These phenotypes suggest that the absence of the FA may reflect the failure of synergid cell differentiation due to incomplete cellularization between the two synergid cells and the central cell (Figure 3, D–F, CC-SY fusion).

In the following experiments, we focused on the single-synergid ovules because they were observed more frequently than the two synergid ovules (Figure 3, C and F). Around the FA, only ~10.0% of the single-synergid ovules produced long plasma membrane invaginations (Figure 3, C and G, greater than ~6 µm), which was considerably fewer than that of normal synergid cells in the wild-type *RHT; ENS* ovules (Figure 3, A and G, 80.9%, n = 377). Next, we performed transmission

electron microscopy to analyze the cell walls at the FA (Figure 3, H–K). In wild-type *RHT; ENS*, the cell walls exhibited a typical finger-like pattern consisting of an electron-dense central region surrounded by a translucent peripheral layer (Figure 3, H and I, 100%, $n = 7$). Similar finger-like cell walls were also observed in the single-synergid ovules of *ProMYB98:PHS1ΔP RHT; ENS* (Figure 3, J and K, 80%, $n = 5$). To investigate the expression and localization of the cytoskeleton and pollen tube attractant, we introduced the microtubule, F-actin, and pollen tube attractant markers into the wild-type *RHT* and *ProMYB98:PHS1ΔP; RHT* lines (Figure 3, L–Q). The single-synergid ovules carrying *ProMYB98:PHS1ΔP* displayed no fibers, visualized using the *ProMYB98:Citrine-TUA5* microtubule marker, confirming the substantial effect of PHS1ΔP expression microtubule depolymerization (Figure 3, L and M). Normal longitudinal F-actin (*ProMYB98:Lifeact-mNeonGreen*) was observed in the single-synergid ovules of the *ProMYB98:PHS1ΔP* line (Figure 3, N and O). Finally, the pollen tube attractant marker, *ProAtLURE1.2:AtLURE1.2-Citrine*, showed a comparable Citrine focus at the FA in both wild-type and *ProMYB98:PHS1ΔP* lines, indicating normal polarized secretion in these ovules (Figure 3, P and Q)., Altogether, these results suggest that whisker-like microtubules facilitate the growth of plasma membrane invaginations but have a limited effect on the formation of the basal structure of the FA and cell polarity.

To investigate pollen tube attraction and fertility, pistils from the wild-type *RHT; ENS* and *ProMYB98:PHS1ΔP; RHT; ENS* lines were pollinated with the non-transgenic Col-0 pollen (Supplemental Figure 4). At one-day-after pollination (1 DAP), pollen tubes were visualized by CongoRed staining. In the wild-type *RHT; ENS* pistils, 97.5% of the ovules received pollen tubes and displayed nuclear proliferation in the endosperm, showing successful pollen tube attraction and fertilization (Supplemental Figure 4A, $n = 360$). Similar fertilization phenotypes were also observed in 49.7% of the ovules from *ProMYB98:PHS1ΔP; RHT; ENS* plants (Supplemental Figure 4B, $n = 338$), which corresponded to the total frequency of the single-synergid and two synergid ovules (Figure 3, B, C and F). The remaining 50.3% of ovules did not proliferate the endosperm nuclei (Supplemental Figure 4, C–E and G), implying fertilization abnormalities in these ovules, which also showed no plasma membrane accumulation at the FA (Figure 3, D–F). In the *ProMYB98:PHS1ΔP; RHT; ENS* plants, normal seed development was observed in ∼70% at 10 DAP (Supplemental Figure 4, H–J), which were comparable to the ovules receiving a pollen tube at 1 DAP (Supplemental Figure 4, F and K). Thus, the subset of the PHS1ΔP-expressing ovules might show fertilization soon after pollen tube reception (Supplemental Figure 4, C and F, 22,2%) and would be gradually fertilized by 8 DAP. Although the mechanism of gradually increasing fertility is unclear, these data at least indicate that the loss of long invaginations in the single-synergid cell by PHS1ΔP-mediated microtubule depolymerization would not abolish pollen tube attraction and reception by the synergid cell.

Expression of a dominant-negative form of actin in the synergid cell causes a severe defect in pollen tube attraction

To examine the roles of F-actin in the synergid cell, we generated transgenic plants expressing wild-type ACTIN8 (*WT-ACTIN*) or the dominant-negative form of ACTIN8 (*DN-ACTIN*) from the *MYB98* promoter. Homozygous plants were not recovered in four independent *ProMYB98:DN-ACTIN* lines, implying reduced fertility in the female gametophyte. To further investigate this possibility, we compared 8 DAP seeds in pistils from Col-0 wild-type plants and *ProMYB98:DN-ACTIN* hemizygous mutants pollinated with Col-0 wild-type pollen (Figure 4, A–C). Wild-type pistils contained almost full sets of seeds (Figure 4, A and C). However, approximately half of the seeds remained undeveloped in the *ProProMYB98:DN-ACTIN* line (Figure 4, B and C). Next, we analyzed the hygromycin resistance in these F_1 siblings. Hygromycin resistance in the *ProMYB98:WT-ACTIN* hemizygous line was 52.7%, suggesting normal inheritance in the *ProMYB98:WT-ACTIN* plants from the female gametophyte (Figure 4D). By contrast, hygromycin resistance in the four *ProMYB98:DN-ACTIN* hemizygous lines ranged from 2.8% to 9.5% (Figure 4D). When wild-type Col-0 pistils were pollinated with pollen from the *ProMYB98:WT-ACTIN* or *ProMYB98:DN-ACTIN* hemizygous plants, no reproductive abnormalities, such as reduced seed set or decreased hygromycin resistance, were observed in the F_1 siblings (Figure 4, C and E). Taken together, we concluded that *ProMYB98:DN-ACTIN* caused sterility exclusively in the female gametophyte.

To further investigate the cause of female sterility, we first examined pollen tube attraction. Pistils from wild-type and *ProMYB98:DN-ACTIN* plants were pollinated with wild-type Col-0 pollen, and the pollen tube growth pattern was analyzed at 1 DAP using CongoRed staining. In wild-type pistils, 96.2% of the ovules received the pollen tube, indicative of successful pollen tube attraction (Figure 4, F and H, $n = 227$), whereas pollen tube attraction was observed only in 51.3% of the ovules from the *ProMYB98:DN-ACTIN* line (Figure 4, G and H, $n = 463$). Therefore, *ProMYB98:DN-ACTIN* may reduce ovule fertility through a pollen tube guidance defect.

Loss of F-actin in the synergid cell impairs secretion of pollen tube attractant peptides

The pollen tube attraction defect observed in *ProMYB98:DN-ACTIN* may be explained by a decrease in the secretion of pollen tube attractant peptides from the synergid cell. To assess this hypothesis, we compared the immunostaining pattern of AtLURE1.2 in mature ovules from non-transgenic Col-0, *myb98* homozygous, and *ProMYB98:DN-ACTIN* hemizygous plants (Supplemental Figure 5). AtLURE1.2 signals were detected on the surface of the micropyle and/or funiculus in ∼90% of the ovules from non-transgenic Col-0 plants (Supplemental Figure 5A; $n = 206$). The AtLURE1.2 signal
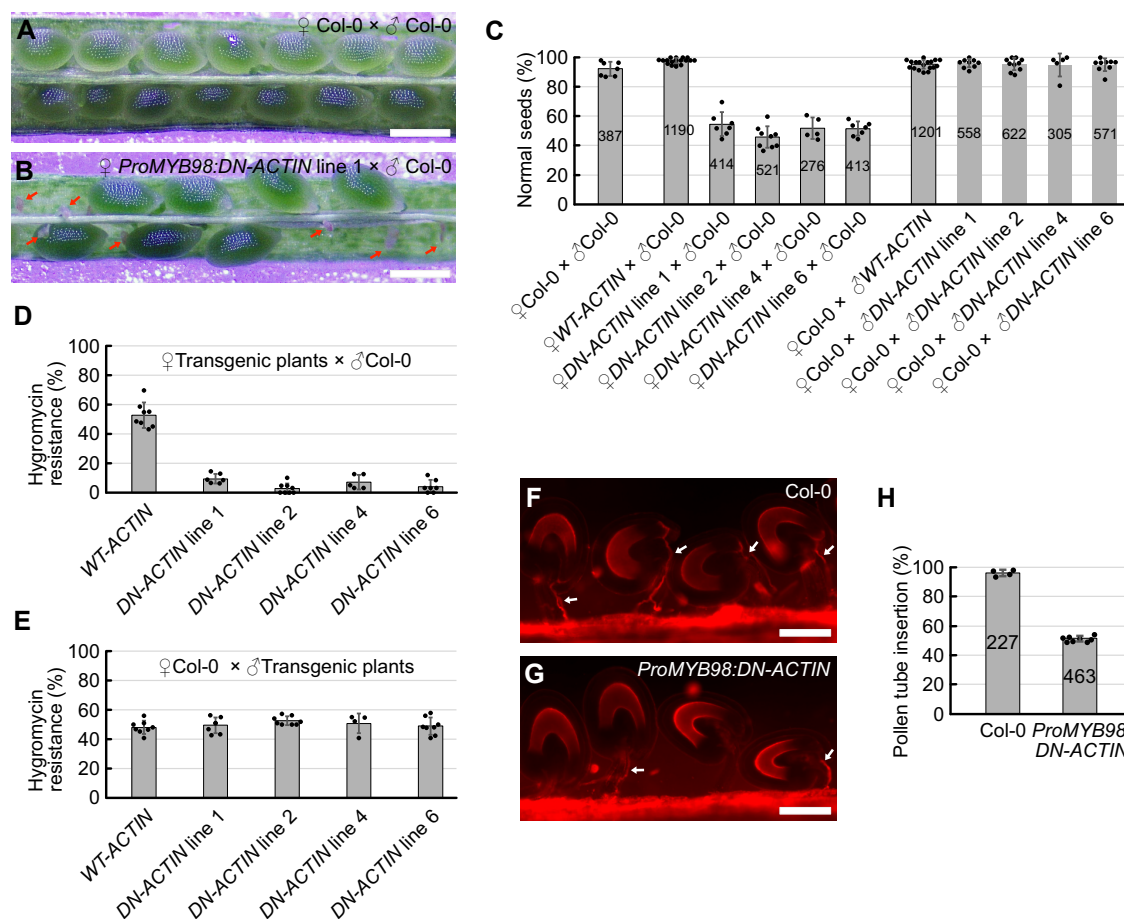
Figure 4 F-actin is required for pollen tube attraction. A, B, Representative images of developing seeds in pistils from wild-type Col-0 plants (A), and *ProMYB98:DN-ACTIN* hemizygous lines (B), analyzed at 8 days after pollination with wild-type Col-0 pollen. Red arrows indicate undeveloped ovules. C, Percentages of normal seeds harvested from pistils after various combinations of cross-pollination among wild-type Col-0 plants, *ProMYB98:WT-ACTIN* hemizygous plants (*WT-ACTIN*), and *ProMYB98:DN-ACTIN* hemizygous plants (*DN-ACTIN*). D, E, Transmission of *ProMYB98:WT-ACTIN* and *ProMYB98:DN-ACTIN* transgenes via the female gametophyte (D) or male gametophyte (E). Gene transmission was analyzed by frequencies of hygromycin-resistant F1 siblings generated by cross-pollination in (B). F, G, Pollen tube growth pattern in pistils from wild-type Col-0 (F) and *ProMYB98:DN-ACTIN* hemizygous (line 1) (G) plants. Pistils were pollinated with wild-type Col-0 pollen and the pollen tubes were visualized by CongoRed staining at one-day-after pollination. White arrows indicate pollen tubes. H, Percentages of pollen tube-inserted ovules analyzed in (F) and (G). Data in (C-E, H) represent the mean ± SD of the points which mean the percentage of seeds or ovules per pistil. Numbers in the bars indicate total seeds or ovules.. Scale bars: 0.5 mm in (A) and (B); 100 μm in (F) and (G).

was below the detection level in the *myb98* homozygous mutant, as reported previously (Supplemental Figure 5B; $n = 231$; Takeuchi and Higashiyama, 2012). In the *ProMYB98:DN-ACTIN* hemizygous plant, AtLURE1.2 signals were only observed in ~40% of the ovules (Supplemental Figure 5C; $n = 260$), indicating a reduction of AtLURE1.2 secretion in the *DN-ACTIN* expressing ovules. To further examine pollen tube attractants in the synergid cells, we used a translational fusion reporter of *AtLURE1.2* and *Citrine* (*ProAtLURE1.2:AtLURE1.2-Citrine*). Consistent with the previous report, the fluorescent signal of AtLURE1.2-Citrine was specifically observed in the synergid cell with the strongest signal detected at the FA (97.0%, $n = 339$; Figure 5, A, B and G; Takeuchi and Higashiyama, 2012). In the *ProMYB98:DN-ACTIN* hemizygous plants that were homozygous for *ProAtLURE1.2:*

AtLURE1.2-Citrine, Citrine signal was detected in 92.9% of ovules ($n = 432$; Figure 5, C–D), suggesting that DN-ACTIN had little effect on gene expression in the synergid cell. However, a normal AtLURE1.2-Citrine secretion pattern was observed only in 46.3% of ovules (WT; Figure 5, C, D and G). In the remaining ovules that were expected to carry *ProMYB98:DN-ACTIN*, AtLURE1.2-Citrine did not accumulate at the FA but rather was uniformly distributed in the cytoplasm (*ProMYB98:DN-ACTIN*; Figure 5, E and F). Abnormalities were also observed in the central vacuole. Wild-type ovules presented a single large central vacuole at the chalazal side (Figure 5, B and D), whereas ovules from the *ProMYB98:DN-ACTIN* hemizygous line often contained multiple small vacuoles located in the middle or micropylar side of the synergid cell (Figure 5F). In agreement, similar
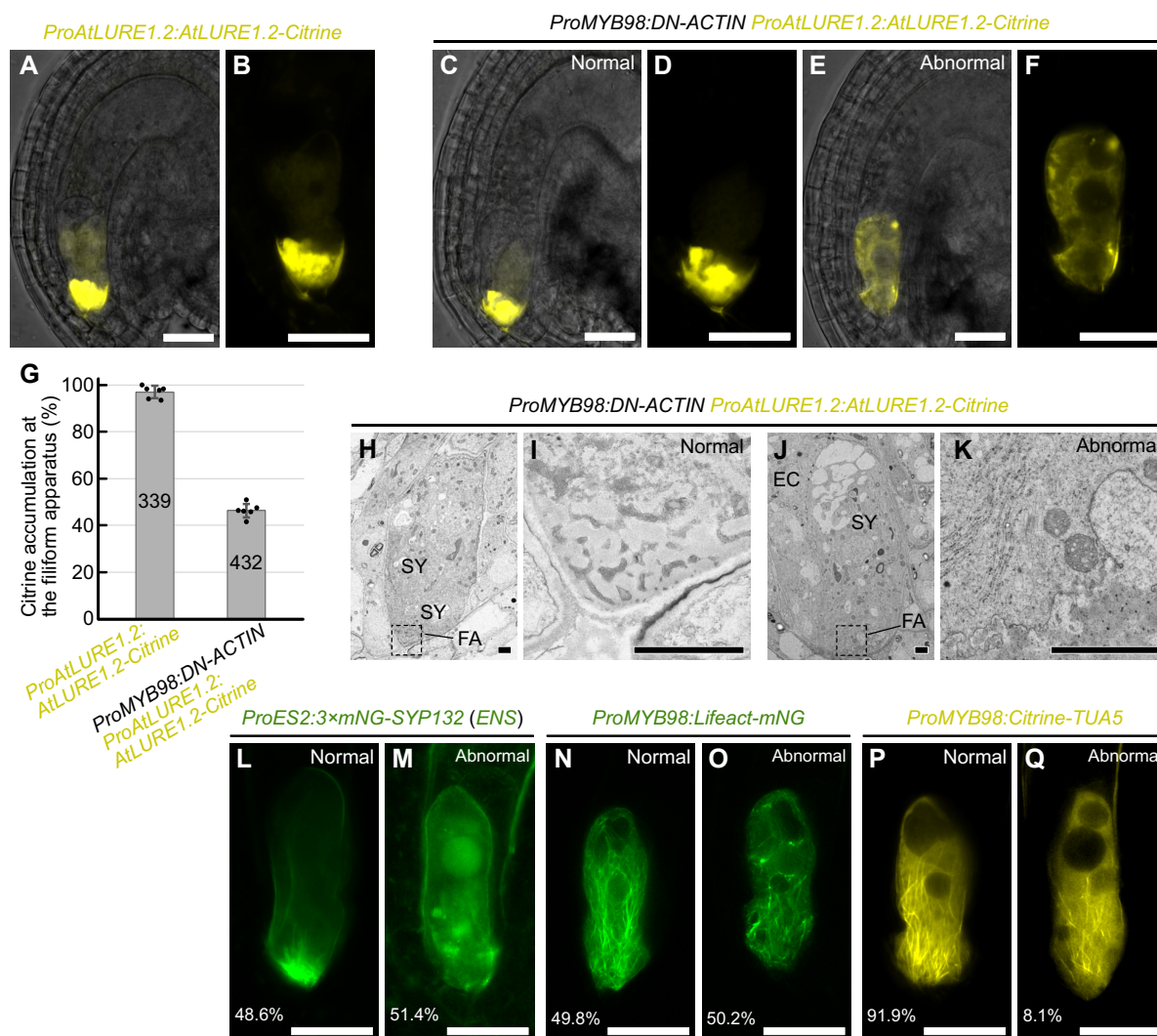
Figure 5 F-actin is necessary for directional protein secretion in synergid cells. A–F, Fluorescent signals of *ProAtLURE1.2:AtLURE1.2-Citrine* pollen tube attractant marker in wild-type (A, B) and *ProMYB98:DN-ACTIN* hemizygous (line 1) (C–F) plants. Merges of fluorescent images and differential interference contrast images are shown in (A), (C), and (E). Fluorescent images of magnified synergid cells are shown in (B), (D), and (F). The *ProMYB98:DN-ACTIN* hemizygous plant showed segregation of wild-type like ovules with a normal fluorescent pattern (C, D), and abnormal ovules with little AtLURE1.2-Citrine signal at the FA (E, F). G, Frequency of ovules displaying normal AtLURE1.2-Citrine accumulation at the FA analyzed in (A) to (F). Data in (D) represent the mean ± SD of the points which mean the percentage of ovules per pistil. Numbers in the bars indicate total ovules. H–K, Transmission electron micrographs of wild-type (H, I) and abnormal (J, K) ovules segregated in pistils from a *ProAtLURE1.2:AtLURE1.2-Citrine* transgenic plant hemizygous for *ProMYB98:DN-ACTIN* (line 1). Magnification of FA indicated by dashed boxes in (H) and (J) are shown in (I) and (K), respectively. L–Q, Confocal images of synergid cells expressing plasma membrane marker (*ProES2:3×mNG-SYP132*; L, M), F-actin marker (*ProMYB98:Lifeact-mNG*; N, O), and microtubule marker (*ProMYB98:Citrine-TUA5*; P, Q) in the *ProMYB98:DN-ACTIN* hemizygous plants (line 1). Representative images of wild-type ovules (L, N, P) and aberrant ovules (M, O, Q; $n = 436, 315, 247$, respectively) are shown. Abbreviations: FA, filiform apparatus; SY, synergid cell; EC, egg cell. Scale bars: 20 μm in (A) to (F) and (L) to (Q); 2 μm in (H) to (K).

results were obtained with the pollen tube attractant marker, *XIUQIU4-Citrine* (Supplemental Figure 6). These data indicate the aberrant secretion of AtLURE1.2 and XIUQIU4 in the DN-ACTIN expressing synergid cells.

We next analyzed the ultrastructure of normal and abnormal ovules segregated from *pMYB98:DN-ACTIN* hemizygous plants that were homozygous for *ProAtLURE1.2:AtLURE1.2-Citrine* (Figure 5, H–K). Although normal ovules with a strong Citrine signal at the FA showed a sponge-like porous domain

of cell walls (Figure 5, H and I; $n = 7$), abnormal ovules had a severely impaired porous cell wall pattern and accumulated electron-dense cell wall materials with a chaotic pattern (Figure 5, J and K; $n = 5$). To examine other morphological aspects of the abnormal synergid cell, marker genes for the plasma membrane and cytoskeleton were introduced into DN-ACTIN expressing lines. In the *ProMYB98: DN-ACTIN* hemizygous plants that were homozygous for *ProES2:3×mNG-SYP132* (ENS), 48.6% of the ovules exhibited

a normal FA pattern, characterized by the accumulation and invagination of mNeonGreen-labeled plasma membrane at the FA (Figure 5L; $n = 436$). The remaining ovules (51.4%) did not have a mNeonGreen focus at the micropylar end, and vesicles of various sizes were detected inside the synergid cell (Figure 5M), suggesting disorganization of the FA in the *ProMYB98:DN-ACTIN* line. In the *ProMYB98: DN-ACTIN* hemizygous plants that were homozygous for *pMYB98:Lifeact-mNeonGreen*, 49.3% of the ovules produced longitudinally aligned F-actin as wild-type ovules observed in Figure 2 (Figure 5M; $n = 319$), while the remaining ovules showed fragmented F-actin and destruction of the actin cable alignment (Figure 5M). On the other hand, typical whisker-like microtubule extensions at the FA did not change between normal and abnormal ovules in the *ProMYB98:DN-ACTIN* hemizygous plants that were homozygous for *ProMYB98:Citrine-TUA5* (Figure 5, P and Q; $n = 212$). The, Citrine-TUA5 pattern indicates independence of F-actin formation and microtubule formation in the synergid cell.

The analyses of the *ProMYB98:DN-ACTIN* transgenic lines revealed important roles of F-actin in pollen tube attraction. However, this genetic approach could not clarify whether the pollen tube attraction defect was induced by the loss of the FA or inhibition of attractant peptide secretion. Thus, we examined changes in synergid cell morphology within a few hours after actin polymerization inhibition by Latrunculin A (LatA) treatment. First, we confirmed that half-an-hour treatment with 100 μM LatA diminished F-actin in the synergid cell from the *ProMYB98:Lifeact-mNG* line (Figure 6, A and B). Interestingly, the *ProMYB98:Citrine-TUA5* synergid cell displayed normal whisker-like microtubule extensions after a 100 μM LatA treatment (Figure 6, C and D), indicating independent regulation of F-actin and microtubules in the synergid cell. In addition, plasma membrane accumulation and invaginations at the FA visualized with *ProES2:3×mNG-SYP132* were not altered even 4 h after 100 μM LatA treatment (Figure 6, E and F). Nevertheless, drastic alterations were observed in the *ProAtLURE1.2:AtLURE1.2-Citrine* line, which showed a Citrine signal focused at the FA in control DMSO-treated ovules that disappeared 4 h after 100 μM LatA treatment, which also induced the appearance of smaller vacuoles (Figure 6, G and H). The LatA-mediated AtLURE1.2-Citrine signal alterations resembled the phenotypes induced by the genetic F-actin destruction in the *ProMYB98:DN-ACTIN* lines (Figure 5, E and F), suggesting that F-actin destruction quickly stalls AtLURE1.2-Citrine secretion in synergid cells even in the presence of a functional FA. A similar analysis was performed by treating *ProAtLURE1.2: AtLURE1.2-Citrine*, *ProES2:3×mNG-SYP132*, *ProMYB98: Lifeact-mNG*, and *ProMYB98:Citrine-TUA5* lines with the microtubule polymerization inhibitor, Oryzalin (Supplemental Figure 7). However, an altered fluorescent pattern was observed only with the *ProMYB98:Citrine-TUA5* microtubule marker (Supplemental Figure 7, C and D). Taken together, these results suggest that F-actin regulates the polarized secretion of pollen tube attractant peptides at the FA.

Longitudinal F-actin disappears temporarily in the persistent synergid cell after pollen tube discharge

Cumulative evidence supporting F-actin-mediated pollen tube attraction prompted us to investigate the F-actin pattern in the persistent synergid during fertilization because it may be involved in the cessation of pollen tube attraction observed after successful double fertilization (Beale et al., 2012; Kasahara et al., 2012). Pistils from *ProMYB98:Lifeact-mNG* were pollinated with pollen from a sperm cell-specific nuclear marker *ProHTR10:HTR10-mRFP1* (Ingouff et al., 2007), and ovules were analyzed by spinning disk confocal microscopy at 6 h after pollination (6 HAP) (Figure 7, A–I). In the unfertilized ovules, a normal longitudinal F-actin pattern was observed in both intact synergid cells on different focal planes (Figure 7, A, E and I). By contrast, a different F-actin pattern was observed in two synergid cells after pollen tube reception. According to the sperm nuclei-derived mRFP1 signals, fertilization states of these ovules were classified into three categories: before plasmogamy, before karyogamy, and after karyogamy. Ovules before plasmogamy contained sperm cells in close proximity to each other, between the egg cell and central cell (Figure 7, B and F). In the ovules before karyogamy, each separated sperm nucleus was observed in the egg cell and central cell (Figure 7, C and G). In ovules after karyogamy, the sperm-derived mRFP1 signal was dispersed in the zygote nucleus or primary endosperm nucleus by chromatin decondensation in ovules after karyogamy (Figure 7, D and H). Throughout these fertilization stages, actin cables were unclear in the receptive synergid and the fluorescent proteins leaked into and marked the boundary of the egg cell and central cell (Figure 7, B–D). In addition, we often observed mNeonGreen foci around the chalazal end of the receptive synergid, which may correspond to the "actin corona" visualized by Rhodamine-phalloidin staining in tobacco (*Nicotiana tabacum*) ovules (Russell, 1993; Huang and Russell, 1994). When the pistils from *ProMYB98:Lifeact-mNG* were fertilized by tagRFP-expressing pollen tubes (*ProLAT52:tagRFP*), we found moderate colocalization of cytosolic tagRFP with the actin corona-like structure (Supplemental Figure 8).

In contrast to the receptive synergid, the persistent synergid did not show actin corona-like structures and the actin cables disappeared before plasmogamy (Figure 7, F and I; $n = 31$). The percentage of ovules containing visible actin cables slightly increased at the stage before karyogamy (Figure 7, G and I; 34%, $n = 38$), and finally reached 58% after karyogamy (Figure 7, H and I; $n = 85$). To examine whether actin cable recovery depended on plasmogamy, we used *gcs1*, a T-DNA insertion allele of *GENERATIVE CELL SPECIFIC 1/HAPLESS2* that produces plasmogamy-defective sperm cells (Mori et al., 2006; von Besser et al., 2006). Pistils from *ProMYB98:Lifeact-mNG* were pollinated with pollen from *gcs1* heterozygous plants carrying *ProHTR10:HTR10-mRFP1*, and the F-actin pattern in the persistent synergid was analyzed in ovules containing unfused sperm cells at 6, 9, and 14 HAP (Figure 7, J and K). At 14 HAP, clear actin cables were observed in the ovules more
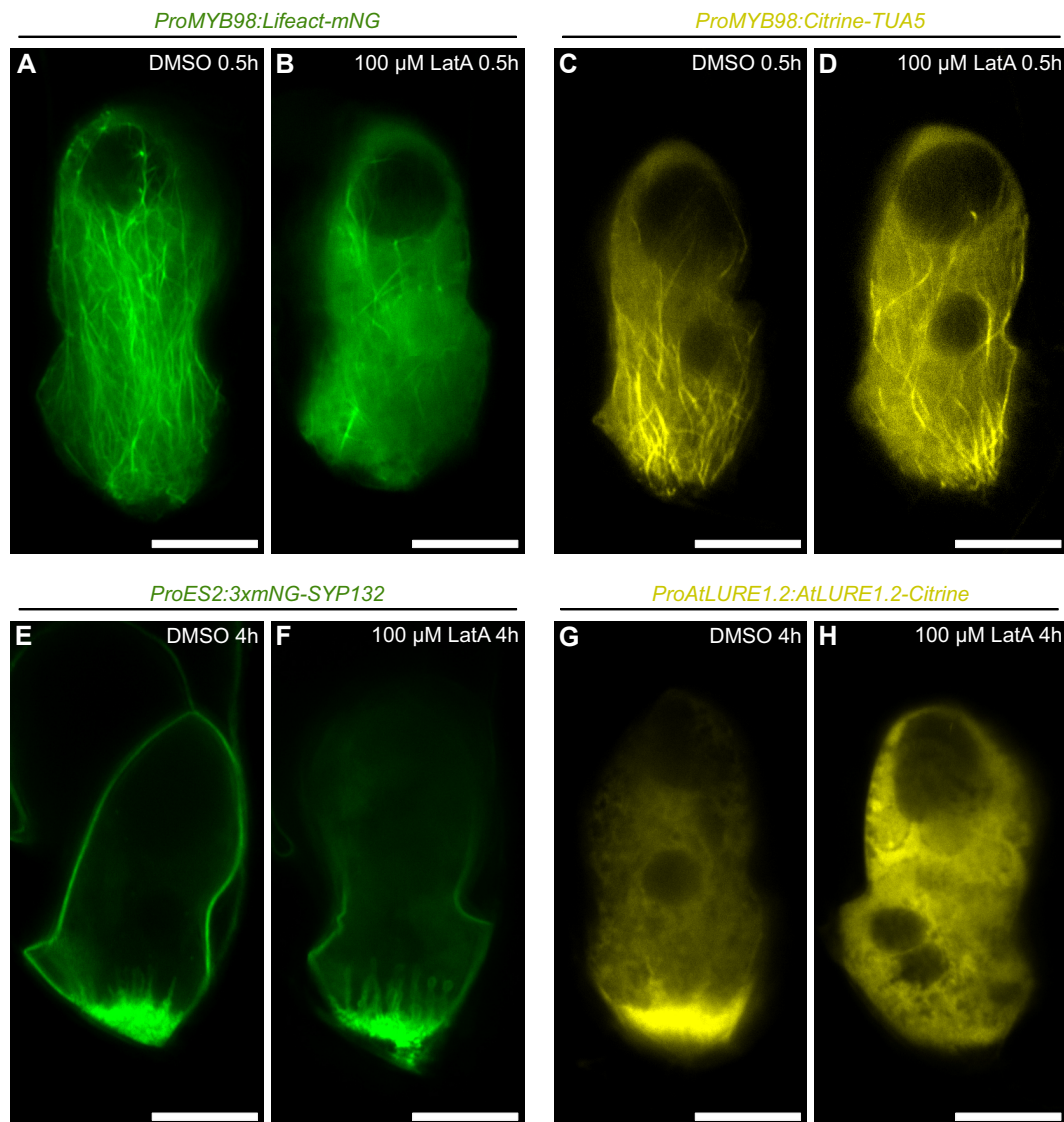
Figure 6 Transient actin depolymerization inhibits AtLURE1.2 accumulation without degeneration of the FA. A–H, Confocal images of synergid cells in *ProMYB98:Lifeact-mNG* (F-actin marker line) (A, B), *ProMYB98:Citrine-TUA5* (microtubule marker line) (C, D), *ProES2:3×mNG-SYP132* (plasma membrane marker line) (E, F), and *ProAtLURE1.2:AtLURE1.2-Citrine* (pollen tube attractant marker line) plants (G, H), cultured in a control medium containing 0.4% DMSO (A, C, E, G), or a medium containing 0.4% DMSO and 100 μM Latrunculin A (LatA) (B, D, F, H). Duration of the ovule culture is shown in the top-right. Scale bars: 20 μm.

frequently than at earlier HAP time points (Figure 7K), indicating the fertilization-independent nature of actin cable recovery. To elucidate the regeneration process of actin cables, we next performed time-lapse imaging. Pistils from *ProMYB98: Lifeact-mNG* were pollinated with pollen from *gcs1/+; ProHTR10:HTR10-mRFP1*, and 6 HAP ovules cultured in a liquid medium were observed every 15 min by spinning disk confocal microscopy. In fertilized ovules, persistent synergids were absorbed by the endosperm within a few hours and the F-actin pattern was no longer visible due to the rapid dilution of Lifeact-mNeonGreen (Supplemental Movie 6). By contrast, ovules containing unfused sperm cells maintained the mNeonGreen signal in the persistent synergid through the 12 h of time-lapse observation (Figure 7L; Supplemental Movie 7). In these unfertilized ovules, few actin cables emerged ~3 h after observation and the actin cables gradually increased in number. These results indicate that pollen tube discharge induces temporal actin depolymerization and cell-autonomous regeneration of actin cables in the persistent synergid.

Discussion

The synergid cell has been extensively studied as the key regulator of the initial communication between male and female gametophytes during fertilization in flowering plants.
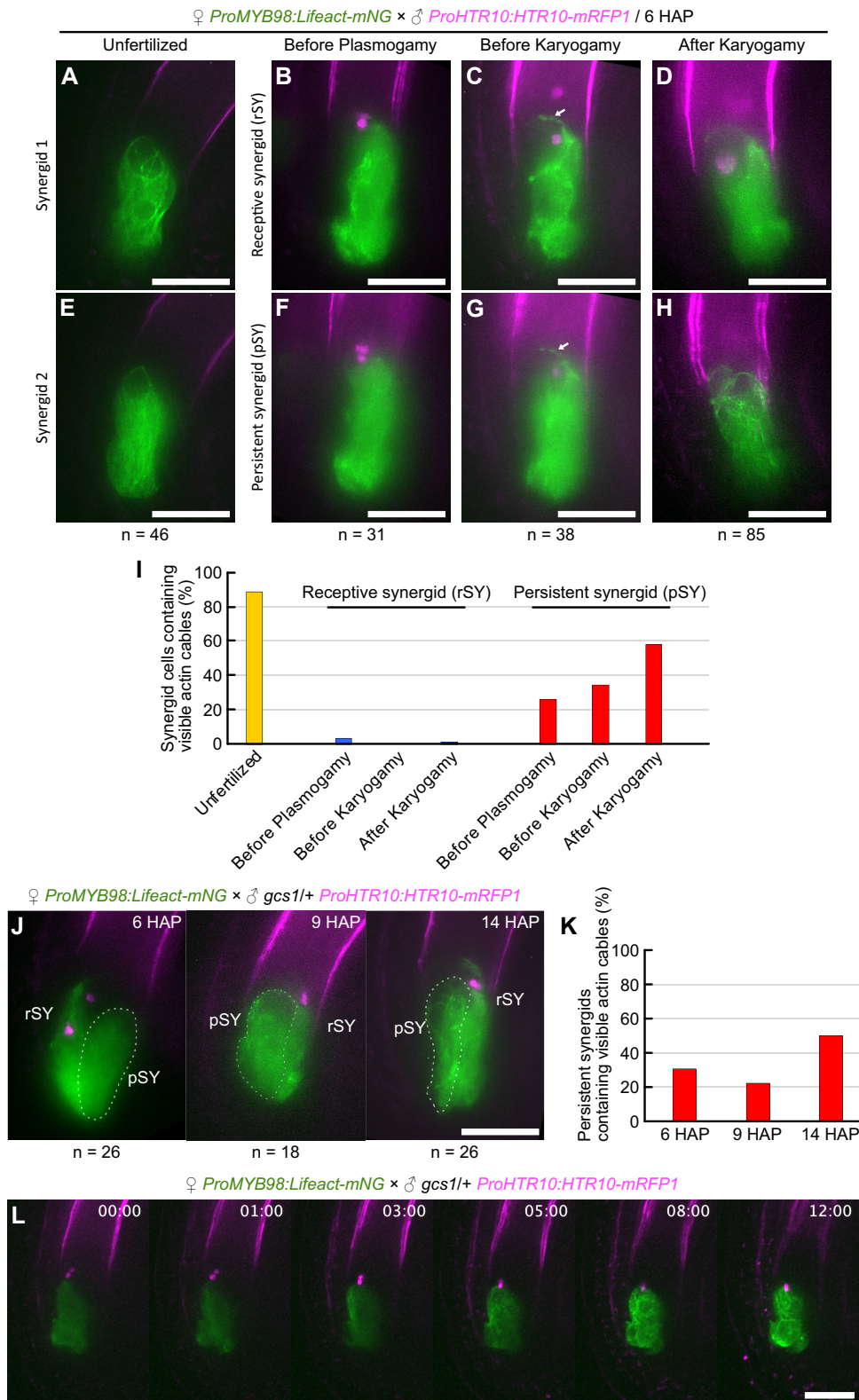
Figure 7 Destruction and reconstruction of F-actin in the persistent synergid. A–I, F-actin pattern in synergid cells during fertilization. Pistils from the *ProMYB98:Lifeact-mNG* F-actin marker line were pollinated with pollen from the *ProHTR10:HTR10-mRFP* sperm nuclear marker line and the ovules were analyzed at 6 h after pollination (6 HAP) by spinning disk confocal microscopy. Images were maximum intensity projections of synergid cells on different focal planes in each Z-series of ovule at the unfertilized stage (A, E), before the plasmogamy stage (B, F), before the karyogamy stage (C, G), and after the karyogamy stage (D, H). The arrows represent the corona-like structure (C, G). After pollen tube reception, receptive synergids (rSY) (B, C, D) can be distinguished from persistent synergids (pSY) (F, G, H) by Lifeact-mNG leakage between the egg cell and central cell.

(continued)

In this study, genetic and pharmacological approaches advanced our understanding of the different roles of microtubules and F-actin in the morphology and functions of synergid cells. Although partial colocalization of microtubules and actin cables was observed in the synergid cell, F-actin disruption did not affect microtubule pattern and *vice versa* (Figures 2, 3, 5 and 6; Supplemental Figure 2 and 7). These observations imply independent functions of the two cytoskeletal components in the synergid cell. Indeed, different phenotypes were observed after disruption of microtubule or F-actin formation. Inhibition of microtubule formation by PHS1ΔP expression led to shorter plasma membrane invaginations at the FA, whereas the ovules accomplished pollen tube attraction and fertilization normally (Figure 3; Supplemental Figure 4). On the other hand, F-actin deformation compromised the polarity of synergid cell organelles and impaired the secretion of pollen tube attractants from the FA (Figures 5 and 6). In a previous report, *ProES2:DN-ACTIN* ovules indicated the misspecification of the egg cell and the synergid cell (Sun et al., 2021). In this study, we detected AtLURE1.2-Citrine and XIUQIU4-Citrine signals specifically in the synergid cells of almost all ovules, although their protein localization patterns were severely impaired. This result suggests that the expression of DN-ACTIN did not disrupt synergid cell identity when using the *MYB98* promoter. Therefore, we propose that longitudinal actin cables play a central role in the formation and maintenance of cell polarity, while microtubules have subsidiary roles in FA formation.

Our FIB-SEM and confocal microscopy analyses revealed a detailed sponge-like FA structure consisting of plasma membranes and cell walls (Figure 1). The porous cell wall pattern was severely impaired by the expression of DN-ACTIN (Figure 5), suggesting that the proper cell wall pattern at the FA requires coordination of actin-mediated protein secretion and cell wall formation. The loss of plasma membrane accumulation was also observed in the PHS1ΔP-expressing ovules, probably due to the incorporation of two synergid cells into the central cell (Figure 3; Supplemental Figure 3 and Movie 5). What are the functions of this widely conserved synergid structure? The role of complex plasma membrane invaginations at the FA may not be confined to only surface expansion of the protein secretion area. Perhaps, the porous cell walls serve as a sponge for the temporary storage of signaling molecules to ensure efficient reproduction. For example, this putative signal storage might support accurate pollen tube attraction by buffering fluctuations of protein secretion. Alternatively, it may modulate pollen tube behavior through the release of a large amount of signaling molecules when the growing pollen tube tip pushes the FA before pollen tube discharge (Higashiyama et al., 1998; Leshem et al., 2013; Ngo et al., 2014).

Not only pollen tube attractant peptides, but also various pollen tube reception factors such as FERONIA, ANJEA, HERK1, LORELEI, and NORTIA are localized at the plasma membrane of the FA (Escobar-Restrepo et al., 2007; Capron et al., 2008; Kessler et al., 2010; Tsukamoto et al., 2010; Galindo-Trigo et al., 2020). NORTIA is relocated from a Golgi-associated compartment to the FA during pollen tube reception, implying cargo-dependent spatiotemporal control of polarized protein secretion in the synergid cell. Polarized protein secretion has been extensively studied in tip-growing model cells including the pollen tube, root hair cell, protonema in mosses, and filamentous fungi (Stephan, 2017; Bibeau et al., 2018). In these cells, F-actin is often concentrated beneath the tip region forming the actin fringe, which facilitates the accumulation of secretory vesicles and subsequent control of polarized secretions crucial for tip-growth (Stephan, 2017). Although F-actin concentration was not obvious around the FA, their active rearrangement may be involved in polarized protein secretion as actin fringes in tip-growing cells.

The movement toward the FA was another feature of F-actin dynamics observed in the synergid cell. This is considerably different from actin dynamics in the egg cell and central cell, where actin cables emerge from the cell periphery and move toward the nucleus (Kawashima et al., 2014; Ohnishi et al., 2014; Ohnishi and Okamoto, 2015). The nucleopetal movement in the female gametes is regulated by an Arp2/3-independent WAVE/SCAR actin nucleation pathway activated by ROP small GTPase and is important for the migration of sperm nuclei after plasmogamy (Ali et al., 2020). Although the female gametophyte cells are originated from the same cell lineage, their functions, morphology, and gene expression are quite different at maturity. Therefore, the synergid cell may present its actin dynamics controlled by a different set of actin modifiers including ROP, Arp2/3, WAVE/SCAR, Formins, and other actin-binding proteins. The F-actin regulator SCAR2 controls F-actin meshwork movement in the central cell and possibly in the egg cell (Ali et al., 2020). In our previous study, the synergid cells in the *myb98* mutant, lacking extensive invaginations characteristic of the FA, have partially egg cell-like gene expression and nuclear position. In the *myb98* synergid cell, slight upregulation in *SCAR2* expression (Susaki et al., 2021) supports the hypothesis of cell-specific regulation of actin in the female gametophyte cells.

Figure 7 (Continued)
The graph shows the percentage of synergid cells containing visible actin cables (I). J–L, F-actin pattern of the persistent synergids in the ovules after reception of fertilization-defective *gcs1* sperm cells. Pistils from *ProMYB98:Lifeact-mNG* plants were pollinated with pollen from a *gcs1* heterozygous plant carrying the *ProHTR10:HTR10-mRFP* marker. Confocal images of ovules before plasmogamy at 6, 9, and 14 h after pollination (J), and percentages of persistent synergids containing visible actin cables (K). Time-lapse imaging of an ovule dissected from a pistil at 6 h after pollination (L). Scale bars: 20 μm.

In our observation, F-actin pattern in the synergid cell changes drastically during fertilization. After pollen tube discharge, fine actin cables disappeared in the ruptured receptive synergid and the synergid-derived Lifeact-mNeonGreen signal appeared as an actin corona (Figure 7). Actin corona was discovered by a Rhodamine-phalloidin staining to observe actin cables around discharged sperm cells prior to double fertilization in tobacco (Russell, 1993; Huang and Russell, 1994). Due to its characteristic spatiotemporal pattern, the actin corona was speculated to transport the released sperm cells to the area where double fertilization takes place. However, live imaging of double fertilization revealed direct delivery of sperm cells from the pollen tube to the position of plasmogamy within a few seconds, implying the existence of an actin-independent sperm cell delivery mechanism in *A. thaliana* (Hamamura et al., 2011). After plasmogamy, actin cables in the female gamete surround the incorporated sperm nucleus to form an aster structure that facilitates sperm nuclear migration toward the female nucleus (Kawashima et al., 2014). The aster structure is morphologically and topologically different from the actin corona reported in tobacco ovules. In this study, we found the actin corona-like accumulation of the Lifeact-mNeonGreen signal exhibited moderate colocalization with cytosolic tagRFP released from the pollen tube (Supplemental Figure 8). The actin corona may be an ephemeral cytosol accumulation irrelevant to sperm cell migration.

The persistent synergid displayed temporal disappearance of actin cables after pollen tube discharge, which may pause secretion of pollen tube attractant peptides and be involved in the mechanisms controlling polytubey block (Maruyama and Higashiyama, 2016). Polytubey block is completed by the degeneration of the persistent synergid triggered by double fertilization. The degeneration processes include a cell fusion between the persistent synergid and endosperm (Maruyama et al., 2015) and degeneration of the persistent synergid nucleus, which is mediated by the EIN3 and EIL1 transcription factors (Völz et al., 2013; Heydlauff et al., 2022; Li et al., 2022) and FIS-class polycomb repressive complex (Maruyama et al., 2013, 2015). Compared to these late degeneration processes, the disappearance of actin cables may be an earlier and fertilization-independent alteration that temporarily inactivates persistent synergid functions (Figure 7, F and I–K). Recent reports have demonstrated several early polytubey block pathways that diminish the attractant signals around the micropyle. Specifically, FERONIA-dependent NO production accompanied by deposition of de-esterified pectin inactivates AtLURE1 peptides via post-translational nitrosation upon pollen tube arrival (Duan et al., 2020). Active AtLURE1 peptides are further reduced by ECS1 and ECS2, which are egg cell-specific aspartic endopeptidases secreted immediately after plasmogamy (Yu et al., 2021). Together with these attractant peptide elimination systems, inhibition of protein secretion in the persistent synergid should play a key role in the early polytubey block. Termination of AtLURE1 secretion and intracellular accumulation of AtLURE1 in the synergid cell are also induced by elevation of NO signaling during pollen tube arrival (Duan et al., 2020). Although the precise mechanism is still unknown, the NO-mediated termination of AtLURE1 secretion may be controlled by the temporal destruction of actin cables. Further studies using inhibitors and mutants affecting NO production and F-actin formation are required to confirm this hypothesis.

Interestingly, the persistent synergid displayed actin cable regeneration, which was more evident in unfertilized ovules after reception of the plasmogamy-defective *gcs1* mutant pollen tube (Figure 7L). When the first pollen tube fails to fertilize the female gametes, the ovules stop the degeneration of the persistent synergid and begin to attract a second pollen tube within ~5 h (Kasahara et al., 2012; Duan et al., 2020; Zhong et al., 2022). The time window between the arrival of the first and second pollen tubes coincides with the period of actin cable disappearance in the persistent synergid, suggesting that actin cable dynamics of destruction–reconstruction function as a courtship-pause timer allowing the persistent synergid to attract the second pollen tube. Occasionally, polytubey causes polyspermy, which might provide the offspring with agronomically useful traits inherited from three parents (Grossniklaus, 2017; Nakel et al., 2017; Mao et al, 2020). To increase the efficiency of such polyspermy breeding, cell biology of persistent synergid reactivation would become important in the future. Our discovery of actin cable regeneration could be the first step toward understanding the molecular mechanism of persistent synergid reactivation.

Materials and methods

Plant materials and growth conditions

Columbia-0 (Col-0) was used as the wild-type strain. The *gcs1* heterozygous mutant that was also homozygous for *ProHTR10:HTR10-mRFP* has been described previously (Kasahara et al, 2012). Seeds were surface sterilized with sterilization solution (2% (v/v) PLANT PRESERVATIVE MIXTURE ^{TM}, 0.1% (v/v) Tween 20), incubated at 4°C for several days, and sown on Murashige and Skoog (MS) medium containing 1% (w/v) sucrose and appropriate antibiotics. Approximately 10 days after germination, plants were transferred to soil. Plants were grown at 22°C under continuous light or standard long day conditions at an optical density of 75 $\mu mol\ m^{-2}\ s^{-1}$ with light-emitting diode (LED) (WPRW01; TOMY DIGITAL BIOLOGY CO., LTD., Japan).

Plasmids and transgenic plants

The *ProRPS5A:H2B-tdTomato* plasmid was kindly provided by D. Kurihara (Nagoya Univ.) (Maruyama et al., 2013). pDM286, a pGWB501 destination vector (Nakagawa et al., 2007) containing the *MYB98* promoter, has been reported previously (Maruyama et al., 2015). The *ProAGL80:tagRFP-TUA5*, pDM230 (a binary vector carrying the *ProLAT52:tagRFP*) and the pSNA128 (a pGWB501 destination vector containing 1,062 bp directly upstream of the coding region of the *ES2*

[At1g26795] (Pagnussat et al, 2007; Hwang et al., 2019)) were gifts from Shuh-ichi Nishikawa (Niigata Univ.). The primers used for plasmid constructions are listed in Supplemental Table 1.

The *PHS1ΔP*, a mutant gene of C-terminus-truncated PROPYZAMIDE-HYPERSENSITIVE 1 (85−700 a.a.) (Fujita et al., 2013), was amplified from Arabidopsis seedling cDNA by PCR using primers "PHS1dP_F + SalI-TOPO" and "PHS1dP_R + AscI-stop", and introduced into the pENTR/D-TOPO vector (Invitrogen) to generate the HTv1243. An LR recombination between pDM286 and HTv1243 produced pDM580, a binary vector containing *ProMYB98:PHS1ΔP*.

HTv1313 and HTv1316, two pollen tube attractant reporter plasmids were cloned as follows. The coding sequence of yellow fluorescent protein Citrine was introduced into the pPZP211 vector by replacing mRuby2 of pPZP211Ru (Takeuchi and Higashiyama, 2016), resulting in pPZP211Cit. The entire genomic sequence of *AtLURE1.2*, including the protein-coding and upstream promoter sequences, was amplified from Arabidopsis genomic DNA by PCR using primers "AtLURE1.2_F + SalIGA" and "AtLURE1.2_-stopR + AscIGA", and introduced into the SalI/AscI site of pPZP211Cit to produce HTv1313, a binary vector harboring *ProAtLURE1.2:AtLURE1.2-Citrine*. Similarly, the entire genomic sequence of CRP810_2.3/XIUIQIU4/TIC3 was amplified by PCR using primers "810_2.3_F + SalIGA" and "810_2.3_-stopR + AscIGA", and introduced into the SalI/AscI site of pPZP211Cit to produce HTv1316, a binary vector harboring *XIUQIU4:XIUQIU4-Citrine*.

To generate the synergid cell-specific F-actin reporter genes, a DNA fragment of *mNeonGreen-* or *mRUBY3*-tagged *Lifeact* was amplified by PCR using primers "pENTR LifeActFP_F" and "FP_R" and cloned into pENTR/D-TOPO to produce pOR099 or pOR102. LR recombination between pDM286 and pOR099 produced pDM522, a binary vector containing *ProMYB98:Lifeact-mNG*, and LR recombination between pDM286 and pOR102 produced pDM523, a binary vector containing *ProMYB98:Lifeact-mRUBY3*.

To generate the synergid cell-specific microtubule reporter gene, a DNA fragment of *mTFP1* was amplified by PCR using primers "pENTR_CFP_F" and "FP_PstI_R" and cloned into pENTR/D-TOPO. Then, the *TUA5* sequence in *ProAGL80:tagRFP-TUA5* was introduced into the NcoI/PstI site of the *mTFP1*-containing entry vector to produce pOR103. The *Citrine* coding sequence was amplified from HTv1313 by PCR using primers "pENTR_cacc_XFP_F" and "FP_PstI_R", and substituted with *mTFP1* in pOR103 by NcoI/PstI digestion and subsequent ligation to generate pOR177. LR recombination between pDM286 and pOR177 produced pDM680, a binary vector containing *ProMYB98:Citrine-TUA5*.

Plasma membrane markers were constructed as follows. pOR084, an entry clone containing *mRUBY2-SYP132*, was constructed using the NEBuilder HiFi DNA Assembly Cloning Kit (New England Biolabs, MA, USA) by multi-DNA fragment assembly between (i) *mRUBY2*-containing pENTR/D-TOPO (Thermo Fisher Scientific, MA, USA) plasmid backbone

amplified by a primer set "FP_SpeI_F" and "FP_EcoRI_R" and (ii) *SYP132* (At5g08080) cDNA sequence amplified by a primer set "SYP132_EcoRI_F" and "SYP132_SpeI_R". pENTR/D-TOPO plasmid backbone with *SYP132* was amplified from pOR084 by PCR using primers "GFP_1-18_R" and "XFP_C-term_F". The resulting linearized plasmid DNA was mixed with three mNeonGreen DNA fragments independently amplified using the "GFP F" and "Linker1_XFP_R", "Linker1_XFP_F" and "Linker2_XFP_R", or "Linker2_XFP_F" and "FP_R" primer sets, and multi-DNA fragment assembly by the NEBuilder HiFi DNA Assembly Cloning Kit was performed to produce pOR129. LR recombination of pSNA128 and pOR129 generated *ProES2:3×mNG-SYP132*. LR recombination of pDM286 and pOR129 generated *ProMYB98:3×mNG-SYP132*. Two plasmids containing wild-type *ACTIN8* (At1g49240) or a dominant-negative mutant of *ACTIN8* (Kato et al., 2010) downstream of the *MYB98* promoter, were constructed by LR recombination between pDM286 and the entry clones carrying wild-type or dominant-negative *ACTIN8*, as described in previously (Kawashima et al., 2014).

Agrobacterium-mediated plant transformation was performed by the floral dipping method using Agrobacterium strain GV3101 (Clough and Bent, 1998). Transformants were selected on MS medium containing 50 μg ml^{-1} hygromycin B or 50 μg ml^{-1} kanamycin. A T3 generation homozygous *ProES2:3×mNG-SYP132* (ENS) plant was cotransformed with *ProRPS5A:H2B-tdTomato* (RHT) and *ProMYB98:PHS1ΔP*. We selected each three independent lines of *ENS; RHT; ProMYB98:PHS1ΔP* by strong genetic linkage or *ENS; RHT*, respectively. A plant with a representative expression pattern of fluorescent protein was selected from each of the three lines and used to generate T3 generation homozygous plants. Three independent lines of *ProMYB98:Citrine-TUA5*, *ProMYB98:Lifeact-mNG*, *ProAtLURE1.2:AtLURE1.2-Citrine* were generated. Representative T2 hemizygous plants generated from these lines were crossed with T3 homozygous *ENS; RHT; ProMYB98:PHS1ΔP* or *ENS; RHT*. F1 plants that lacked *ENS* were selected. Four independent lines of *ProMYB98: Lifeact-mNG; ProMYB98:Citrine-TUA5* were generated and a line with a representative expression pattern of the fluorescent protein was selected. Six independent lines of *ProMYB98:DN-ACTIN* were generated and the line showing an intermediate phenotype with reduced fertility was selected. This line was crossed with *ProMYB98:Citrine-TUA5*, *ProMYB98:Lifeact-mNG*, *ProAtLURE1.2:AtLURE1.2-Citrine*, and *ProXIUQIU4:XIUQIU4-Citrine* and lines that were hemizygous for *DN-ACTIN* and homozygous for the fluorescent reporter were selected.

Analysis of mature ovules

Pistils were harvested one to two days after emasculation and the carpel walls were removed on a glass slide. Then, the pistils were split in half and mounted on 5% sucrose or an ovule culture medium containing Nitsch basal salt mixture (Duchefa) and 5% trehalose dihydrate (Wako Fujifilm) (Gooh et al., 2015). In pharmacological assays, Latrunculin

A or Oryzalin were dissolved in DMSO to make 25 mM stock solutions and stored at −20°C. These stock solutions were thawed and diluted 250 times by the ovule culture media before use (final concentration, 100 μM). Mature ovules were incubated in these inhibitor-containing media or 0.4% DMSO (negative control), and confocal images were obtained using a Leica SP8 TCS (Leica, Wetzlar, Germany). For time-lapse imaging, ovules were dissected from pistils in a droplet of ovule culture medium containing Nitsch basal salt mixture (Duchefa) and 5% trehalose dihydrate (Wako Fujifilm) (Gooh et al., 2015), and transferred to a glass bottom dish (D141410; Matsunami Glass IND., LTD., Japan). The XY positions of the ovules were recorded by bright field observation, and time-lapse confocal images were captured using an IX73 inverted microscope (Olympus, Tokyo, Japan) equipped with a spinning disk confocal scanning unit (CSU-W1; Yokogawa, Tokyo, Japan) and an sCMOS camera (Zyla 4.2; Andor, Belfast, Northern Ireland).

Analysis of seed phenotypes

Siliques at 8 days after pollination were attached to a glass slide with double-sided tape and the upper side of the carpel walls was removed with an ophthalmic knife. The samples were imaged using a dissecting microscope Leica E4 W (Leica, Wetzlar, Germany). To investigate the frequency of normal seeds, we harvested fully matured siliques and counted normal seeds and undeveloped seeds under a dissecting microscope.

Histochemistry

CongoRed staining was performed as previously described by Kasahara et al. (2005), with slight modifications. Dissected pistils at 1 day after pollination were treated with 0.4% (w/v) CongoRed Solution for 1 min on a glass slide and washed several times with 5% (w/v) sucrose. The signals from fluorescent proteins disappeared once the samples were treated with alkaline aniline blue solution. To observe tdTomato-labeled nuclei and a pollen tube in the same ovule (Supplemental Figure 4, A–E), CongoRed was used as a fluorescent-protein-compatible dye. To unify the pollen tube analysis, we also used CongoRed staining in Figure 4, F and G. ImmunoStaining of AtLURE1.2 was performed as reported previously (Takeuchi and Higashiyama, 2012). These samples were observed using an upright microscope (Axio Imager. M1; Zeiss, Jera, Germany) equipped with filter sets for DsRed or GFP. Epi-fluorescent images of those pistils were captured using an IX73 inverted microscope (Olympus, Tokyo, Japan). Aniline blue staining was performed as previously described by Maruyama et al. (2013). Cell wall staining of the FA was modified from Musielak et al. (2015). Staining solution was 0.1% (v/v) SCRI Renaissance 2200 (SR2200: Renaissance Chemicals; stock solution of the supplier was considered as 100%) diluted in ovule culture medium (Gooh et al., 2015). These samples were observed using a Leica SP8 TCS (Leica, Wetzlar, Germany). Aniline blue and SR2200 were excited with a 405-nm laser and emission was recorded between 410 and 485 nm.

Focused ion beam-scanning electron microscopy

FIB-SEM sample blocks were prepared as follows. Wild-type Col-0 ovules were fixed overnight in a fixation solution (4% paraformaldehyde, 2% glutaraldehyde, 0.05 M cacodylate buffer), and then washed three times with 0.05 M cacodylate buffer. The samples were subjected to postfixation with osmium tetroxide in 0.05 M cacodylate buffer at 4°C for 1 h and washed five times with distilled water. After incubation with 1% thiocarbohydrazide for 20 min and five rounds of washing with distilled water, the ovules were treated with 2% aqueous osmium tetroxide at room temperature for 1 h and washed three times with distilled water. The samples were stained overnight with 1% aqueous uranyl acetate at 4°C, and then treated with 0.03 M lead aspartate at 60°C for 30 min. The tissue was then dehydrated with increasing ethanol concentrations (50%, 70%, 90%, 100%), transferred into propylene oxide, infiltrated, and embedded in Quetol 651. Specimens were analyzed by FIB-SEM as described previously (Oi et al., 2017). Briefly, the surfaces of the embedded ovules were exposed using a diamond knife on an ultramicrotome (EM UC6; Leica, Wetzlar, Germany), and the resin blocks were trimmed to a cuboid and attached to a standard specimen stage for FIB-SEM as the exposed ovules faced the SEM column. The specimens were coated with a thin layer of carbon using a carbon coater (CADE-E, Meiwafosis, Tokyo, Japan) to prevent electron charging. The serial electron micrographs were obtained with a FIB-SEM (MI-4000L, Hitachi, Tokyo, Japan). The FIB was operated with the following conditions: accelerating voltage, 30 kV; beam current for milling to prepare or to cut, 1.6 or 1.2 nA, respectively; cutting interval (z-step), 25 nm. The SEM was operated with the following conditions: accelerating voltage, 1.0 kV; working distance, 2 mm; image size, 2000×2000 pixels; color depth, 8-bit (256 gray scales); pixel size, 25 nm per pixel. Secondary and backscattered electrons were detected by the detector in the SEM column (U + EsB). The images of serial sections were processed using "Fiji" software (http://fiji.sc/Fiji) (Schindelin et al., 2012); gray scale was inverted, brightness and contrast were adjusted, the images were aligned using the "Register Virtual Stack Slices" (Translation-Translation -no deformation) tool, and then the region of the FA was cropped (image size, 400×400 pixels). The outline of cell walls of two synergid cells in all 2D images was traced manually using the software "PaintTool SAI" (ver. 1, Systemax, Japan). The inside region of the two synergid cells was binarized to detect the FA and to reconstruct it into the 3D model using the software "Image-Pro Premier 3D" (ver. 9.3, Media Cybernetics, USA); the surface rendering model was reconstructed with subsampling (64 M voxel) and smoothing (low-pass filter [3:3:3]), and then their surface area was calculated with the function "3D Measure".

Transmission electron microscopy

Emasculated pistils from the transgenic plants homozygous for ProMYB98:PHS1ΔP, ProRPS5A:H2B-tdTomato, and

ProES2:3×mNG-SYP132, were dissected on glass slides and analyzed using an upright microscope (Axio Imager. M1; Zeiss, Jera, Germany) to select the ovules containing a single-synergid cell. Similarly, normal and abnormal ovules were selected from the *ProAtLURE1.2:AtLURE1.2-Citrine* transgenic plant hemizygous for *ProMYB98:DN-ACTIN*. The ovule selection procedure was skipped when we prepared wild-type controls of the cytoskeleton-disrupted transgenic plants. The ovules were fixed in a solution containing 4% paraformaldehyde, 2% glutaraldehyde, and 50 mM sodium cacodylate at pH7.4 for several days at 4°C. The samples were washed in buffer and post-fixed for 6 h in 2% aqueous osmium tetroxide at 4°C. The specimens were then dehydrated in a graded ethanol series, transferred into propylene oxide, infiltrated, and embedded in Quetol 651. Series of thin sections (80 nm) were stained with 2% aqueous uranyl acetate and lead citrate, and examined at 80 kV under a JEOL JEM 1400 Plus electron microscope (JEOL Ltd.). Digital images were taken with a CCD camera (VELETA; Olympus Soft Imaging Solutions).

Analysis of F-actin flow

Time-lapse images of F-actin dynamics in synergid cells expressing *ProMYB98:Lifeact-mNG* were captured by spinning disk confocal microscopy with 30 sec intervals (total 21 frames; 600 sec) and multiple z-planes (total nine planes, 1 μm intervals). The images were deconvoluted using the constrained iterated deconvolution function of CellSens Dimension Desktop 3.2 (Olympus). Background noise was removed using the subtract background function in Fiji (Schindelin et al., 2012). Three z-planes including the peri-nuclear areas of the time-lapse images were projected and then used for analysis of F-actin flow in the synergid cell. To analyze the F-actin flow, flow velocity vectors (v_x, v_y) were obtained from spatiotemporal image correlation spectroscopy analysis using MATLAB (MATLAB Inc.) scripts (Ashdown et al., 2015) with the following parameter settings: pixelSize 0.259, timeframe 30, tauLimit 4, filtering FourierWhole, MoveAverage 21, ROIsize 16, ROIshift 4, TOIsize 3, TOIshift 1 as described in the manual (Ashdown et al., 2015). After the flow velocity vectors were acquired from each analysis area, all angles of the flow velocity vectors from the entire analyzed frames were calculated and normalized as probability using a custom MATLAB script to get direction distribution of the F-actin flow.

Colocalization analysis

Background noise of the images was removed by Gaussian filter and background subtraction functions using Imaris 9.7.2 (BitPlane) prior to colocalization analysis between the F-actin and microtubule channels. Quantification of the colocalization was obtained using the Imaris Coloc function to create the colocalization channel and statistical values including Pearson's and thresholded Manders' coefficient.

Accession numbers

Sequence data from this article can be found in the GenBank/EMBL libraries under the following accession numbers: *MYB98*

(AT4G18770), *ES2* (AT1G26795), *SYP132* (AT5G08080), *HISTONE H2B* (AT1G07790), *PHS1* (AT5G23720), *AtLURE1.2* (AT5G43510), *XIUQIU1* (At5g50423), *XIUQIU4* (At5g48605), *ACTIN8* (AT1G49240), *TUA5* (AT5G19780), *HTR10* (AT1G19890), *myb98-1* (SALK_020263), *gcs1* (SALK_135694).

Supplemental data

The following materials are available in the online version of this article.

Supplemental Figure S1. Confocal images of mature ovules from the *ProES2:3×mNG-SYP132* (*ENS*) plasma membrane marker line.

Supplemental Figure S2. F-Actin flow and colocalization of F-actin and microtubules in synergid cells.

Supplemental Figure S3. Female gametophyte development in *RHT; ENS* and *ProMYB98:PHS1ΔP; RHT; ENS* transgenic homozygous plants.

Supplemental Figure S4. Fertilization of ovules expressing PHS1ΔP in synergid cells.

Supplemental Figure S5. Immunostaining of AtLURE1.2.

Supplemental Figure S6. F-actin is necessary for directional XIUQIU4 secretion.

Supplemental Figure S7. Transient microtubule depolymerization.

Supplemental Figure S8. Moderate colocalization of an actin corona-like structure and pollen tube cytosol.

Supplemental Table S1. Primers used in this study.

Supplemental Movie 1. A 3D image of cell walls at the filiform apparatus reconstructed from serial sections obtained by FIB-SEM.

Supplemental Movie 2. Confocal z-series images of the filiform apparatus in the *ProMYB98:3×mNG-SYP132* plasma membrane marker line.

Supplemental Movie 3. Dynamics of F-actin in a synergid cell of mature ovule.

Supplemental Movie 4. Time-lapse series of female gametophyte development in *RHT; ENS*.

Supplemental Movie 5. Time-lapse series of female gametophyte development in *ProMYB98:PHS1ΔP; RHT; ENS*.

Supplemental Movie 6. F-actin dynamics of persistent synergids in two fertilized ovules.

Supplemental Movie 7. F-actin dynamics of persistent synergids in three unfertilized ovules.

References

Ali MF, Fatema U, Peng X, Hacker SW, Maruyama D, Sun M-X, Kawashima T (2020) ARP2/3-independent WAVE/SCAR pathway and class XI myosin control sperm nuclear migration in flowering plants. Proc Natl Acad Sci U S A 117(51): 32757–32763

Ashdown G, Pandžić E, Cope A, Wiseman P, Owen D (2015) Cortical actin flow in T cells quantified by spatio-temporal image correlation spectroscopy of structured illumination microscopy data. J Vis Exp 2015(106): e53749

Beale KM, Leydon AR, Johnson MA (2012) Gamete fusion is required to block multiple pollen tubes from entering an Arabidopsis ovule. Curr Biol 22(12): 1090–1094

Bibeau JP, Kingsley JL, Furt F, Tüzel E, Vidali L (2018) F-Actin mediated focusing of vesicles at the cell tip is essential for polarized growth. Plant Physiol 176(1): 352–363

Capron A, Gourgues M, Neiva LS, Faure JE, Berger F, Pagnussat G, Krishnan A, Alvarez-Mejia C, Vielle-Calzada JP, Lee YR, et al. (2008) Maternal control of male-gamete delivery in Arabidopsis involves a putative GPI-anchored protein encoded by the LORELEI gene. Plant Cell 20(11): 3038–3049

Clough SJ, Bent AF (1998) Floral dip: a simplified method for Agrobacterium-mediated transformation of Arabidopsis thaliana. Plant J 16(6): 735–743

Diboll AG, Larson DA (1966) An electron microscopic study of the mature megagametophyte in Zea mays. Am J Bot 53(4): 391–402

Dresselhaus T, Sprunck S, Wessel GM (2016) Fertilization mechanisms in flowering plants. Curr Biol 26(3): R125–R139

Duan Q, Liu MJ, Kita D, Jordan SS, Yeh FJ, Yvon R, Carpenter H, Federico AN, Garcia-Valencia LE, Eyles SJ, et al. (2020) FERONIA Controls pectin- and nitric oxide-mediated male-female interaction. Nature 579(7800): 561–566

Eng RC, Sampathkumar A (2018) Getting into shape: the mechanics behind plant morphogenesis. Curr Opin Plant Biol 46: 25–31

Escobar-Restrepo JM, Huck N, Kessler S, Gagliardini V, Gheyselinck J, Yang WC, Grossniklaus U (2007) The FERONIA receptor-like kinase mediates male-female interactions during pollen tube reception. Science 317(5838): 656–660

Fujita S, Pytela J, Hotta T, Kato T, Hamada T, Akamatsu R, Ishida Y, Kutsuna N, Hasezawa S, Nomura Y, et al. (2013) An atypical tubulin kinase mediates stress-induced microtubule depolymerization in Arabidopsis. Curr Biol 23(20): 1969–1978

Galindo-Trigo S, Blanco-Tourinan N, DeFalco TA, Wells ES, Gray JE, Zipfel C, Smith LM (2020) CrRLK1L receptor-like kinases HERK1 and ANJEA are female determinants of pollen tube reception. EMBO Rep 21(2): e48466

Gooh K, Ueda M, Aruga K, Park J, Arata H, Higashiyama T, Kurihara D (2015) Live-cell imaging and optical manipulation of Arabidopsis early embryogenesis. Dev Cell 34(2): 242–251

Grossniklaus U (2017) Polyspermy produces tri-parental seeds in maize. Curr Biol 27(24): R1300–R1302

Hamamura Y, Saito C, Awai C, Kurihara D, Miyawaki A, Nakagawa T, Kanaoka MM, Sasaki N, Nakano A, Berger F, et al. (2011) Live-cell imaging reveals the dynamics of two sperm cells during double fertilization in Arabidopsis thaliana. Curr Biol 21(6): 497–502

Heydlauff J, Serbes IE, Vo D, Mao Y, Gieseking S, Nakel T, Harten T, Völz R, Hoffmann A, Groß-Hardt R (2022) Dual and opposing roles of EIN3 reveal a generation conflict during seed growth. Mol Plant 15(2): 363–371

Higashiyama T, Kuroiwa H, Kawano S, Kuroiwa T (1998) Guidance in vitro of the pollen tube to the naked embryo sac of Torenia fournieri. Plant Cell 10(12): 2019–2031

Huang B-Q, Russell SD (1994) Fertilization in Nicotiana tabacum: cytoskeletal modifications in the embryo sac during synergid degeneration. Planta 194(2): 200–214

Hwang D, Wada S, Takahashi A, Urawa H, Kamei Y, Nishikawa SI (2019) Development of a heat-inducible gene expression system using female gametophytes of Arabidopsis thaliana. Plant Cell Physiol 60(11): 2564–2572

Ingouff M, Hamamura Y, Gourgues M, Higashiyama T, Berger F (2007) Distinct dynamics of HISTONE3 variants between the two fertilization products in plants. Curr Biol 17(12): 1032–1037

Jensen WA (1965) The ultrastructure and histochemistry of the synergids of cotton. Am J Bot 52(3): 238–256

Johnson MA, Harper JF, Palanivelu R (2019) A fruitful journey: pollen tube navigation from germination to fertilization. Annu Rev Plant Biol 70(1): 809–837

Ju Y, Yuan J, Jones DS, Zhang W, Staiger CJ, Kessler SA (2021) Polarized NORTIA accumulation in response to pollen tube arrival at synergids promotes fertilization. Dev Cell 56(21): 2938–2951.e6

Kasahara RD, Maruyama D, Hamamura Y, Sakakibara T, Twell D, Higashiyama T (2012) Fertilization recovery after defective sperm cell release in Arabidopsis. Curr Biol 22(12): 1084–1089

Kasahara RD, Portereiko MF, Sandaklie-Nikolova L, Rabiger DS, Drews GN (2005) MYB98 Is required for pollen tube guidance and synergid cell differentiation in Arabidopsis. Plant Cell 17(11): 2981–2992

Kato T, Morita MT, Tasaka M (2010) Defects in dynamics and functions of actin filament in Arabidopsis caused by the dominant-negative actin fiz1-induced fragmentation of actin filament. Plant Cell Physiol 51(2): 333–338

Kawashima T, Maruyama D, Shagirov M, Li J, Hamamura Y, Yelagandula R, Toyama Y, Berger F (2014) Dynamic F-actin movement is essential for fertilization in Arabidopsis thaliana. Elife 3: e04501

Kessler SA, Shimosato-Asano H, Keinath NF, Wuest SE, Ingram G, Panstruga R, Grossniklaus U (2010) Conserved molecular components for pollen tube reception and fungal invasion. Science 330(6006): 968–971

Leshem Y, Johnson C, Sundaresan V (2013) Pollen tube entry into the synergid cell of Arabidopsis is observed at a site distinct from the filiform apparatus. Plant Reprod 26(2): 93–99

Li C, Yeh FL, Cheung AY, Duan Q, Kita D, Liu MC, Maman J, Luu EJ, Wu BW, Gates L, et al. (2015) Glycosylphosphatidylinositol-anchored proteins as chaperones and co-receptors for FERONIA receptor kinase signaling in Arabidopsis. Elife 4: e06587

Li W, Li Q, Lyu M, Wang Z, Song Z, Zhong S, Gu H, Dong J, Dresselhaus T, Zhong S, et al. (2022) Lack of ethylene does not affect reproductive success and synergid cell death in Arabidopsis. Mol Plant **15**(2): 354–362

Mansfield SG, Briarty LG, Erni S (1991) Early embryogenesis in Arabidopsis thaliana. I. The mature embryo sac. Can J Bot **69**(3): 447–460

Mao Y, Gabel A, Nakel T, Viehöver P, Baum T, Tekleyohans DG, Vo D, Grosse I, Groß-Hardt R (2020) Selective egg cell polyspermy bypasses the triploid block. Elife **9**: e52976

Marton ML, Cordts S, Broadhvest J, Dresselhaus T (2005) Micropylar pollen tube guidance by egg apparatus 1 of maize. Science **307**(5709): 573–576

Marton ML, Fastner A, Uebler S, Dresselhaus T (2012) Overcoming hybridization barriers by the secretion of the maize pollen tube attractant ZmEA1 from Arabidopsis ovules. Curr Biol **22**(13): 1194–1198

Maruyama D, Hamamura Y, Takeuchi H, Susaki D, Nishimaki M, Kurihara D, Kasahara RD, Higashiyama T (2013) Independent control by each female gamete prevents the attraction of multiple pollen tubes. Dev Cell **25**(3): 317–323

Maruyama D, Higashiyama T (2016) The end of temptation: the elimination of persistent synergid cell identity. Curr Opin in Plant Biol **34**: 122–126

Maruyama D, Völz R, Takeuchi H, Mori T, Igawa T, Kurihara D, Kawashima T, Ueda M, Ito M, Umeda M, et al. (2015) Rapid elimination of the persistent synergid through a cell fusion mechanism. Cell **161**(4): 907–918

Meng J-G, Zhang M-X, Yang W-C, Li H-J (2019) TICKET Attracts pollen tubes and mediates reproductive isolation between relative species in Brassicaceae. Sci China Life Sci **62**(11): 1413–1419

Mori T, Kuroiwa H, Higashiyama T, Kuroiwa T (2006) GENERATIVE CELL SPECIFIC 1 is essential for angiosperm fertilization. Nat Cell Biol **8**(1): 64–71

Musielak TJ, Schenkel L, Kolb M, Henschen A, Bayer M (2015) A simple and versatile cell wall staining protocol to study plant reproduction. Plant Reprod **28**(3-4): 161–169

Nakagawa T, Suzuki T, Murata S, Nakamura S, Hino T, Maeo K, Tabata R, Kawai T, Tanaka K, Niwa Y, et al. (2007) Improved gateway binary vectors: high-performance vectors for creation of fusion constructs in transgenic analysis of plants. Biosci Biotechnol Biochem **71**(8): 2095–2100

Nakel T, Tekleyohans DG, Mao Y, Fuchert G, Vo D, Groß-Hardt R (2017) Triparental plants provide direct evidence for polyspermy induced polyploidy. Nat commun **8**(1): 1–8

Ngo QA, Vogler H, Lituiev DS, Nestorova A, Grossniklaus U (2014) A calcium dialog mediated by the FERONIA signal transduction pathway controls plant sperm delivery. Dev Cell **29**(4): 491–500

Ohnishi Y, Hoshino R, Okamoto T (2014) Dynamics of male and female chromatin during karyogamy in rice zygotes. Plant Physiol **165**(4): 1533–1543

Ohnishi Y, Okamoto T (2015) Karyogamy in rice zygotes: actin filament-dependent migration of sperm nucleus, chromatin dynamics, and de novo gene expression. Plant Signal Behav **10**(2): e989021

Oi T, Enomoto S, Nakao T, Arai S, Yamane K, Taniguchi M (2017) Three-dimensional intracellular structure of a whole rice mesophyll cell observed with FIB-SEM. Ann Bot **120**(1): 21–28

Okuda S, Tsutsui H, Shiina K, Sprunck S, Takeuchi H, Yui R, Kasahara RD, Hamamura Y, Mizukami A, Susaki D, et al. (2009) Defensin-like polypeptide LUREs are pollen tube attractants secreted from synergid cells. Nature **458**(7236): 357–361

Pagnussat GC, Yu HJ, Sundaresan V (2007) Cell-fate switch of synergid to egg cell in Arabidopsis eostre mutant embryo sacs arises from misexpression of the BEL1-like homeodomain gene BLH1. Plant Cell **19**(11): 3578–3592

Pereira AM, Nobre MS, Pinto SC, Lopes AL, Costa ML, Masiero S, Coimbra S (2016) Love is strong, and you're so sweet": jAGGER is essential for persistent synergid degeneration and polytubey block in Arabidopsis thaliana. Mol Plant **9**(4): 601–614

Riedl J, Crevenna AH, Kessenbrock K, Yu JH, Neukirchen D, Bista M, Bradke F, Jenne D, Holak TA, Werb Z, et al. (2008) Lifeact: a versatile marker to visualize F-actin. Nat Methods **5**(7): 605–607

Russell SD (1993) The egg cell: development and role in fertilization and early embryogenesis. Plant Cell **5**(10): 1349–1359

Schindelin J, Arganda-Carreras I, Frise E, Kaynig V, Longair M, Pietzsch T, Preibisch S, Rueden C, Saalfeld S, Schmid B, et al. (2012) Fiji: an open-source platform for biological-image analysis. Nat Methods **9**(7): 676–682

Schulz R, Jensen WA (1968) Capsella embryogenesis: the synergids before and after fertilization. Am J Bot **55**(5): 541–552

Shaner NC, Lambert GG, Chammas A, Ni Y, Cranfill PJ, Baird MA, Sell BR, Allen JR, Day RN, Israelsson M, et al. (2013) A bright monomeric green fluorescent protein derived from Branchiostoma lanceolatum. Nat Methods **10**(5): 407–409

Stephan OOH (2017) Actin fringes of polar cell growth. J Exp Bot **68**(13): 3303–3320

Sun Y, Wang X, Pan L, Xie F, Dai B, Sun M, Peng X (2021) Plant egg cell fate determination depends on its exact position in female gametophyte. Proc Natl Acad Sci U S A **118**(8): e2017488118

Susaki D, Suzuki T, Maruyama D, Ueda M, Higashiyama T, Kurihara D (2021) Dynamics of the cell fate specifications during female gametophyte development in Arabidopsis. PLoS Biol **19**(3): e3001123

Takeuchi H, Higashiyama T (2012) A species-specific cluster of defensin-like genes encodes diffusible pollen tube attractants in Arabidopsis. PLoS Biol **10**(12): e1001449

Takeuchi H, Higashiyama T (2016) Tip-localized receptors control pollen tube growth and LURE sensing in Arabidopsis. Nature **531**(7593): 245–248

Tsukamoto T, Qin Y, Huang Y, Dunatunga D, Palanivelu R (2010) A role for LORELEI, a putative glycosylphosphatidylinositol-anchored protein, in Arabidopsis thaliana double fertilization and early seed development. Plant J **62**(4): 571–588

Uemura T, Ueda T, Ohniwa RL, Nakano A, Takeyasu K, Sato MH (2004) Systematic analysis of SNARE molecules in Arabidopsis: dissection of the post-Golgi network in plant cells. Cell Struc Funct **29**(2): 49–65

Völz R, Heydlauff J, Ripper D, von Lyncker L, Groß-Hardt R (2013) Ethylene signaling is required for synergid degeneration and the establishment of a pollen tube block. Dev Cell **25**(3): 310–316

von Besser K, Frank AC, Johnson MA, Preuss D (2006) Arabidopsis HAP2 (GCS1) is a sperm-specific gene required for pollen tube guidance and fertilization. Development **133**(23): 4761–4769

Webb MC, Gunning BES (1994) Embryo sac development in Arabidopsis thaliana II. The cytoskeleton during megagametogenesis. Sex Plant Reprod **7**(3): 153–163

Yu HJ, Hogan P, Sundaresan V (2005) Analysis of the female gametophyte transcriptome of Arabidopsis by comparative expression profiling. Plant Physiol **139**(4): 1853–1869

Yu X, Zhang X, Zhao P, Peng X, Chen H, Bleckmann A, Bazhenova A, Shi C, Dresselhaus T, Sun MX (2021) Fertilized egg cells secrete endopeptidases to avoid polytubey. Nature **592**(7854): 433–437

Zhong S, Li L, Wang Z, Ge Z, Li Q, Bleckmann A, Wang J, Song Z, Shi Y, Liu T, et al. (2022) RALF Peptide signaling controls the polytubey block in Arabidopsis. Science **375**(6578): 290–296

Zhong S, Liu M, Wang Z, Huang Q, Hou S, Xu YC, Ge Z, Song Z, Huang J, Qiu X, et al. (2019) Cysteine-rich peptides promote interspecific genetic isolation in Arabidopsis. Science **364**(6443): eaau9564